UNIVERSITEIT VAN AMSTERDAM

MSc Physics

Track Advanced Matter and Energy Physics

Master Thesis

Silver Nanocubes as Building Blocks for a Transparent Conductive Network

by Annemarie Berkhout
5834937

10 November 2015

60 ECTS

November 2014 - September 2015

Supervisor:
dr. Erik C. Garnett
Daily supervisor:
dr. Beniamino Sciaccca

Second examiners:
prof. dr. Albert Polman
prof. dr. A. Femius Koenderink

Abstract

The realization of metal nanoscale geometries has important applications in sensing, plasmonics and optoelectronics. The fabrication of such nanostructures requires the use of advanced nanofabrication facilities. Lithography techniques allow the fabrication of arbitrary nanopatterns, but the resulting structures are polycrystalline due to the use of thermal evaporation in the metal deposition step. Electrical conductivity in polycrystalline crystal structures is limited, because of electrons scattering from grain boundaries. This issue has been reported for silver nanowire networks by Sciacca et al. [1]. Functional single-crystalline structures can be made alternatively by epitaxially growing metal using expensive techniques such as molecular beam epitaxy, followed by etching into a desired pattern. However, with this process much material is wasted.

Here, we propose a technique to make single-crystalline nanopatterns, via assembly of silver nanocube subunits. Silver is used because of its excellent conductive properties. With a chemical treatment the silver nanocubes can be connected such that a single-crystalline junction is established. Without the need for metal evaporation this technique permits application on a large scale. To demonstrate the concept of single-crystalline nanopatterning, the model geometry under study in this thesis is a transparent electrode grid. We present the synthesis of silver nanocubes, followed by assembly of the particles in a rectangular lattice pattern through a dipcoating process. Using a chemical treatment involving the reducing agent $NaBH_4$ an epitaxial connection between cubes is formed, which is shown by HRTEM. Our experiments provide a new platform for the fabrication of arbitrary single-crystalline patterns.

Contents

Abstract **i**

1 Introduction **1**

2 Synthesis of silver nanocubes **3**
2.1 Theory . . . 3
2.2 Methods . . . 4
2.3 Results . . . 5
2.4 Conclusion . . . 8

3 Assembly **9**
3.1 Introduction . . . 9
3.2 Methods . . . 9
3.3 Results . . . 11
3.4 Conclusion . . . 17

4 Welding **19**
4.1 Introduction . . . 19
4.2 Optical welding . . . 19
4.2.1 532 nm laser . . . 19
4.2.2 Broadband light . . . 22
4.3 Chemical welding . . . 24
4.3.1 Tollens' reagent . . . 24
4.3.2 $NaBH_4$ solution . . . 25
4.3.3 Tollens' reagent: local . . . 27
4.4 Conclusion . . . 28

5 Characterization of interfacial welding **29**
5.1 Introduction . . . 29
5.2 Methods . . . 29
5.3 Results . . . 29
5.4 Conclusion . . . 32

6 Conclusion **33**

Acknowledgements **35**

References **37**

7 Appendix **41**
7.1 Silver nanocube synthesis . . . 41
7.1.1 Materials and chemicals list . . . 41
7.1.2 Reaction conditions and reproducibility . . . 42
7.1.3 Non-cubic results . . . 42
7.1.4 Size distribution of silver nanocubes . . . 44
7.2 Silicon wire template - preliminary result . . . 45

1 Introduction

Silver is the 47th element in the periodic table. Its symbol Ag originates from the Greek $\acute{\alpha}\rho\gamma\upsilon\rho o\varsigma$ and Latin argentum, meaning grey or shining. Silver has remarkable characteristics: it possesses the highest electrical conductivity [2] and the lowest optical losses [3] of all metals. These outstanding properties lead to many applications of silver in plasmonics [4,5], surface enhanced Raman scattering (SERS) detection [6,7], sensing [8,9] and transparent conducting electrodes (TCEs) for optoelectronics [10,11].

TCEs are essential components in optoelectronic devices, such as solar cells, touchscreens and light emitting diodes, since TCEs provide optical transparency and electrical conductivity simultaneously. Indium tin oxide (ITO) is commonly used as transparent conductive layer, however its performance is limited. Additional drawbacks of this material are its costly deposition process and its brittleness. These disadvantages have led to several research alternatives, among which graphene [12,13], carbon nanotubes [14,15], conductive polymers [16] and metal nanowire networks [10,11,17–19].

To maximize the conductivity of nanowire networks, the best metal to use is silver. Silver nanowire networks are shown to perform better than ITO [20] and can additionally be made flexible [19]. Such networks have been realized by the deposition and welding of silver nanowires grown in solution [11,18], however no control over the resulting geometry is achievable with this method. Carefully designing silver nanowire networks by tuning the geometry and thickness of the wires allows the maximization of optical transparency and electrical conductivity. Such ordered nanowire arrays have been made on a large scale using soft conformal imprint lithography (SCIL) [21] by Van de Groep et al. [17], and are shown to outperform the transmittance and sheet resistance of ITO. The downside of nanofabrication using lithography is the need for metal deposition by thermal evaporation. This process is costly, but more importantly it intrinsically results in polycrystalline structures that suffer from increased Ohmic losses. If grain boundaries can be removed, the electric performance of nanowire networks can be greatly improved, and the resistivity of these networks can approach that of bulk silver.

To create a monocrystalline silver grid pattern, our proposal is to utilize a bottom-up fabrication process employing single-crystalline nanocubes as subunits (see figure 1). Single-crystalline nanoparticles can be made in solution via a thermodynamically and kinetically driven growth process [22]. Bottom-up assembly permits the arrangement of nanoparticles in arbitrary geometries, as shown with 50 nm spheres by Cui et al. [23]. For the case of cubes, literature reports assembly in various configurations, including face-face and edge-edge orientation [24], and packing in 2D monolayers [25] and 3D structures [26,27].

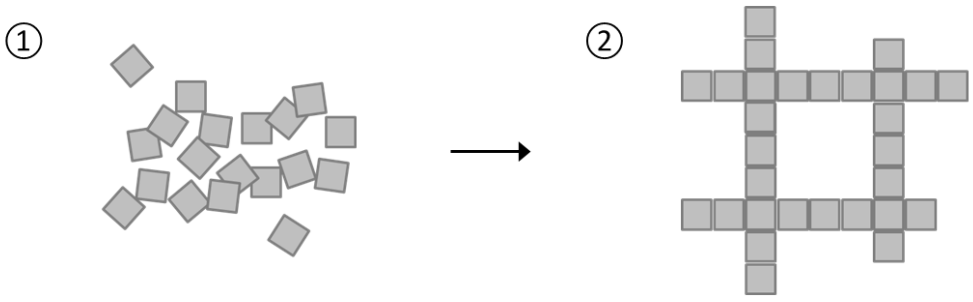

Figure 1: *Silver nanocubes (1) are used as single crystalline building blocks to fabricate a rectangular grid (2). The size of the cubes and the pitch of the grid are not to scale.*

Silver nanocubes have been assembled in lines using Langmuir Blodgett assembly [28], however with this method relatively large gaps remain between the particles, and precise control over the position of the particles is not feasible. Continuous lines of silver nanocubes have, to our knowledge, not been realised yet. For electronic applications of the assembled particles, it is furthermore necessary that, by welding, an electrical connection between the cubes is achieved. During welding the cubes need to maintain their crystal structure and orientation. For a monocrystalline final structure the junction between neighboring cubes has to be epitaxial. Nanoparticle assembly followed by welding for the purpose of single-crystalline patterning has not yet been reported.

The applications of nanoparticle self-assembly and welding are not limited to nanowire networks. With the technique described in this thesis in principle arbitrary single-crystalline silver patterns can be made, facilitating the fabrication of e.g. plasmonic architectures. In addition, metals other than silver (that can be made into cubes) can be employed, such as copper, gold, palladium and platinum.

To fabricate an interconnected silver grid, the approach taken is the following. First, as is described in the next section, silver nanocubes are synthesized using a polyol method [29]. An edge length of 50 nm is aimed, since this is close to the electron mean free path in silver. Next, using a SCIL technique, a flexible mold containing grid-shaped trenches is made, in a shape similar to [20]. With a dip-coating technique [23] the silver cubes are assembled in this grid pattern. A simple transfer method allows the printing of assembled particles on a silicon or quartz substrate. These experiments are shown in section 3. Subsequently, two approaches to weld the silver cubes are examined: optical and chemical. The best welding is obtained with a chemical treatment. Finally, the connection between two chemically welded cubes is characterized using HRTEM, as is presented in section 5.

2 Synthesis of silver nanocubes

To study the feasibility of fabricating conductive nanoscale patterns, first the building blocks are synthesized. This section starts with theory on nanoparticle synthesis, in particular silver nanocubes. The subsequent experimental part reports on the synthesis and characterization of these particles.

2.1 Theory

Nanocrystal growth Metal nanoparticles can be grown in solution from single atoms. The first stage of this growth process is nucleation [30]. Once the concentration of atoms in a solution is above a threshold, atoms start to cluster and form nuclei to decrease the energy of the system. These nuclei continue to grow into larger nanocrystals by the addition of atoms. Once a certain size is reached, structural changes become energetically costly, at which point the crystal structure of the nuclei is fixed to a well-defined shape. These crystals, known as seeds, can take different shapes: single-crystalline, singly twinned and multiply twinned [22]. Generally the nucleation of atoms results in a combination of these differently shaped seeds.

Most metals, including silver, crystallize in a face centered cubic (fcc) structure (see figure 2a). Single-crystalline silver seeds grow in this fcc structure without grain boundaries and are shaped such that the total interfacial free energy as compared to the volume is minimized [31]. As the surface to volume ratio is minimal for a sphere, these seeds are terminated by a combination of {100} and {111} facets (see figures 2b and c), such that they take a truncated octahedron shape. A particle with this morphology, illustrated in figure 2d, is almost spherical.

The single-crystalline, singly twinned and multiply twinned seeds can each grow into differently shaped nanoparticles. For nanoparticle synthesis, the key to obtaining particles with only one morphology (e.g. cubic) is prohibiting the existance of undesired seeds [22], which can be achieved by selectively etching these particles. Once the desired seeds are obtained, the evolution to the final structure can be tuned by using capping agents that steer the growth. Choosing the right parameters seeds can grow into nanoparticles of many different shapes: cubes, octahedra, bars, rods, wires, bipyramids, plates etcetera.

Growth into cubes Nanocubes grow from a single crystalline seed. To acquire mainly seeds with this morphology, a silver nanocube synthesis generally includes HCl or HNO_3 to selectively etch the non single-crystalline seeds. For the evolution to a cubic structure, the

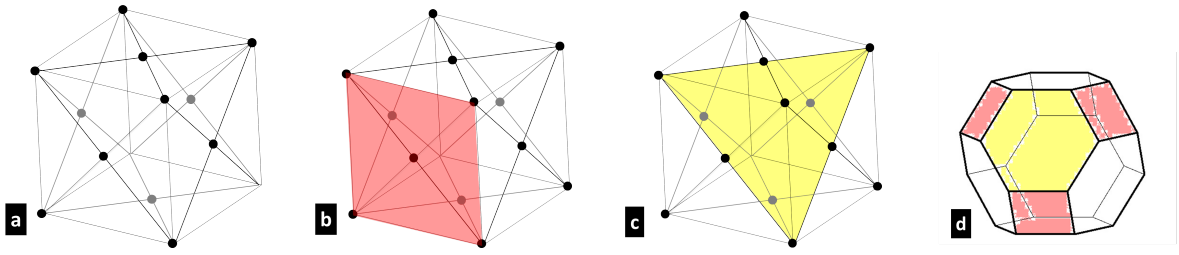

Figure 2: a: *Schematic image of a face centered cubic (FCC) crystal structure.* **b:** *The* {100} *crystal plane shown in red.* **c:** *The* {111} *crystal plane shown in yellow.* **d:** *Schematic image of a truncated octahedron. The red and yellow facets are the* {100} *and* {111} *planes respectively. If a nanoparticle with this shape grows in the* ⟨111⟩ *direction it will take a cubic shape.*

seeds (terminated by both {100} and {111} facets) need to be terminated with {100} facets only. To promote this specific termination a capping agent such as polyvinylpyrrolidone (PVP) is used. PVP shows different binding affinities with different crystallograpic planes of silver: the {100} and {111} plane of a silver seed have a different surface atom density which causes PVP to bind more strongly to the {100} facets. This induces silver atoms to bind preferentially to the {111} facets (the yellow facets in figure 2d). Silver adheres to all planes of a crystal such that the crystals grow in every direction, increasing in size. However, by growing preferentially in the ⟨111⟩ direction, the crystals get terminated by {100} facets only, resulting in cubes [32].

Nanocube synthesis Silver nanocubes can be synthesized with a polymer mediated polyol synthesis [29,33,34]. Such a reaction involves the reduction of silver ions by a polyol (e.g. ethylene glycol (EG)) at elevated temperature, where the polyol additionally serves as the solvent for the precursor containing silver. To avoid clustering of colloidal particles and to promote the formation of cubes, the polymer capping agent PVP is required.

Although many reports on the fabrication of silver nanocubes use $AgNO_3$ as the silver precursor [32–34], here cubes were obtained using CF_3COOAg [29]. Apart from CF_3COOAg, EG and PVP, this reaction includes trace amounts of NaSH and HCl. NaSH is reported to be necessary to form Ag_2S clusters, that catalyze the reduction of CF_3COOAg [35]. HCl is added to the reaction to remove the non single-crystalline seeds. Cl^- ions and O_2 together are a strong oxidizing agent [22, 36]. Since twinned seeds have more defects than single crystalline seeds, these twinned seeds are oxidatively etched selectivily. This leaves mainly single crystalline seeds which is essential for the formation of cubic nanoparticles.

2.2 Methods

Silver nanocubes are synthesized following Zhang et al. [29] using egg shaped magnetic stir bars (recommended by Skrabalak et al. [33]) and 12 mL vials with a diameter of 23 mm. The experimental procedure is described next. A list of reagents and equipment needed is included in the Appendix (section 7.1.1).

Preparation Ten vials (of which four containing a stir bar) and the beakers are cleaned the day before use, with diluted aqua regia consisting of d.i.water, HCl (37% in water) and HNO_3 in a 4 : 3 : 1 ratio. All the cleaned glassware is left in a drying oven overnight and taken out just before use. For each synthesis four reactions are carried out at the same time, varying the concentration of HCl. This was done to compare results using different concentration of HCl.

As soon as the vials have cooled down to room temperature, a rubber ring is put around the reactions vials for placement in a custom made vial holder. Each vial is filled with 5 mL of ethylene glycol (EG) and put in an oil bath on top of a hotplate. The heating and stirring are then switched on (150°C, rotation speed 300 RPM). It takes less than half an hour to reach this temperature, during which the reagents are freshly prepared.

For four vials, first 150 mg PVP is dissolved in 6 mL EG, giving a concentration of 25 mg mL^{-1} in EG. The latter is transferred to the vial first to prevent PVP from sticking to the flask wall. While the PVP is dissolving (promoted by using a vortex) the other reagents can be prepared. A 0.06 mM solution of NaSH is made by dissolving 5.04 mg NaSH in 10 mL EG and diluting this with a factor three. The HCl solution is prepared by

adding 24.7 μL HCl to 10 mL EG. To obtain a concentration of 3 mM this solution must be diluted ten times. Taking smaller amounts of HCl would increase the error in the initial volume taken. Finally, a solution of 282 mM CF_3COOAg in EG is prepared by mixing 124.6 mg CF_3COOAg with 2 mL EG. The dissolution of all reagents is promoted using a vortex (no sonication).

Reaction Once the EG in the reaction vials has reached 150°C, and all reagents have dissolved, the reaction can start. Usually this is one hour after introducing the reaction vials to the oil bath. First, 30 μL of NaSH is added to each reaction vial. Two minutes later HCl is added to the four vials (for example 0.5, 0.75, 1.0 and 1.5 mL, corresponding to 0.21, 0.30, 0.39 and 0.55 mM HCl in the reaction). At t = 4 minutes, 1.25 mL of PVP is introduced. Finally, at t = 5.5 minutes, 400 μL CF_3COOAg is added. After adding the silver precursor the loosely fitting caps are placed on top of the vials.

60 minutes after adding CF_3COOAg the reaction is quenched by putting the vials in an ice bath. When ending a reaction after 45 minutes, high quality cubes will have formed, yet slightly smaller. Acetone is added to the vials to remove excess PVP from the reaction mixture, and these suspensions are transferred to four centrifuge tubes. After centrifugation (20 to 30 min at 5000 RPM) the transparent white/yellow supernatant is poured out. Next, water is added up to 5 mL followed by 1 mL ethanol to decrease the contact angle of the liquid (in order to remove the supernatant more easily). The suspension is mixed using a vortex, then centrifuged for 30 min at 5000 RPM. After pouring out the supernatant, this cleaning step is repeated three times. Finally, one cleaning with ethanol is done and the final product is suspended in ethanol.

In order to characterise the result of the synthesis in an electron microscope, a few μL of the nanocube suspension is dropcast on a piece of silicon. After drying the sample is immersed in acetone and then in isopropylalcohol (IPA) (30 seconds each) to remove residual organics. The samples are imaged using a scanning electron microscope (SEM, FEI Verios 460) at voltages of 5-10 kV.

2.3 Results

Reaction colors Quickly after the silver precursor has been added, a slight yellow color is observed in the reaction mixture. For the 0.39 mM HCl reaction after roughly three minutes the yellow color shifts to orange. A hint of pink is seen in most reactions prior to orange. For four reactions with different HCl concentrations, all shifts in color during the reaction are delayed for higher HCl concentration: the color changes are seen first in the reaction with the lowest HCl concentration. After becoming orange the reaction mixture will darken to olive/green/brown (in between these stages hints of red are also observed occasionally). At the same time the suspension becomes more opaque. For the 0.39 mM HCl reaction this is around 9 minutes after introducing CF_3COOAg. After these color changes mainly the opacity increases and the reactions start looking more greyish. The final product looks olive/green/brown/grey, the exact color varies with concentrations of HCl. All reactions that yielded cubes show a yellow reddish meniscus and silver looking plating on the stir bars (see figures 3a and b). If the multi color meniscus was absent the reaction did not yield cubes. If, upon cleaning with nitric acid, the stir bars remained greyish, silverchloride particles had formed. Examples of results other than cubes are shown in section 7.1.3 in the Appendix.

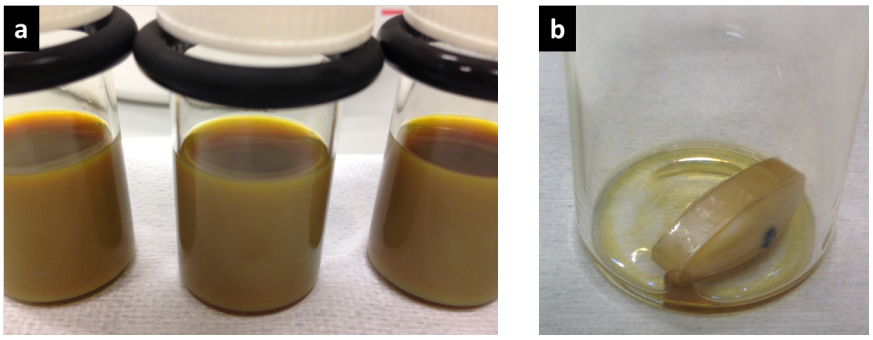

Figure 3: a: *The yellow/red meniscus seen at the end of a reaction that yielded (among other shapes) cubes.* **b:** *The silver plating visible on the stirring bar if a reaction succeeded.*

Nanocubes Silver nanocubes have been synthesized following the described procedure using HCl concentrations in the range of 0.2 to 0.55 mM. Multiple syntheses were conducted keeping all parameters and the HCl concentration constant, but since both shape and size of the resulting particles were seen to vary (see figure 27 in the Appendix), an optimal HCl concentration could not be determined.

The result of a silver nanocube synthesis using 0.39 mM HCl is shown in figure 4a. It shows not only cubes but also wires and larger non-cubic silver particles, which is typical for all our syntheses. By fine tuning the procedure one might be able to decrease the amount of undesired particles, though these particles can be easily removed. By centrifuging the nanoparticle suspension (using a Hettich Universal 320 centrifugator) the bigger particles precipitate, leaving cubes and wires on top as shown in figure 4b. This sample was centrifuged for 60 min at 800 RPM, but separation of particles can be done quicker by increasing the centrifugation speed. Removing wires is done by filtering the nanoparticle suspension with 450, 220 and 100 nm teflon pores subsequently (using Merck millipore, durapore membrane filters). This yields mostly cubes, as can be seen in figure 4c. Investigating the 100 nm filter showed that a relatively large number of cubes stuck to this membrane, while most wires had already been removed by the 220 nm filter. Therefore, for most reaction mixtures filtering with 450 and 220 nm pores is sufficient.

In view of filtering, it is interesting to note that when a suspension of cubes was stored

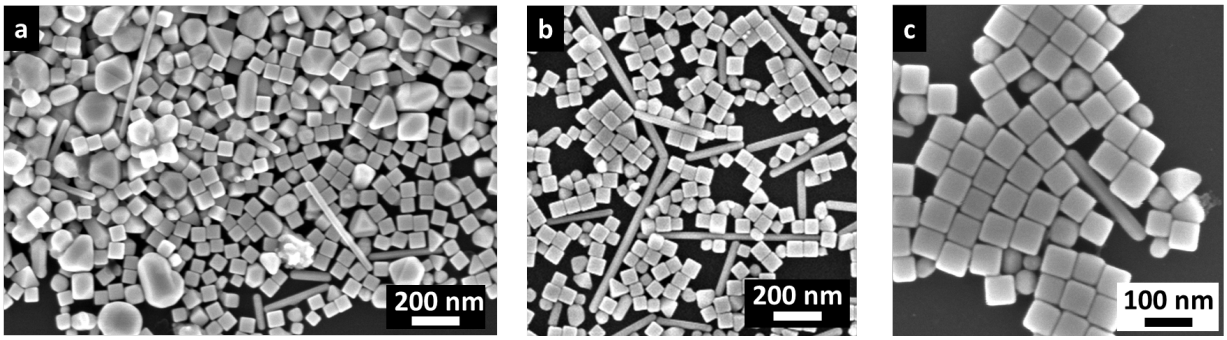

Figure 4: a: *Result of the silver nanocube synthesis described in the Methods (HCl concentration 0.39 mM). The undesired wires and larger particles can be removed by centrifuging and filtering.* **b:** *The supernatant of the reaction result after centrifuging: the larger particles have precipitated out.* **c:** *After filtering the centrifuged batch with 450, 220 and 100 nm pores subsequently, mostly cubic nanocrystals are left.*

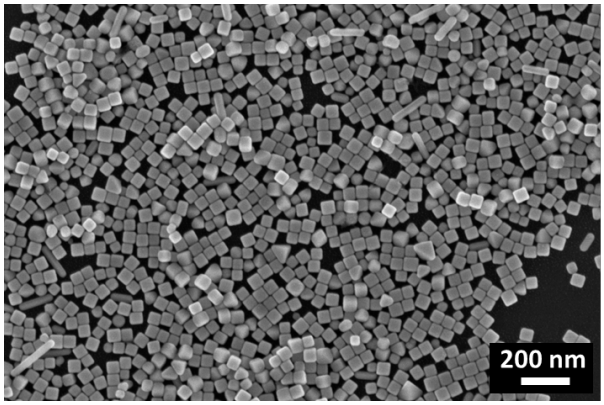

Figure 5: *A suspension of cubes in ethanol after several months: size-selective precipitation has occurred, leaving monodispersed cubes in the suspension.*

for several months, size-selective precipitation was observed (see figure 5). The larger, heaviest particles had precipitated to the bottom, leaving a monodispersed suspension.

Characterization The size distribution of the synthesized nanocubes is calculated from SEM images using the imaging program ImageJ. Figure 6 shows such a size distribution for a synthesis with a reaction time of 48 minutes. The average cube length is 41.6 nm, a standard deviation σ of 6.2 nm is calculated in Mathematica. For counting, the SEM images were converted to black and white images. This conversion induced a slight underestimation of the sizes (see also figure 30 in the Appendix). Larger cubes can be obtained by extending the reaction time of the synthesis.

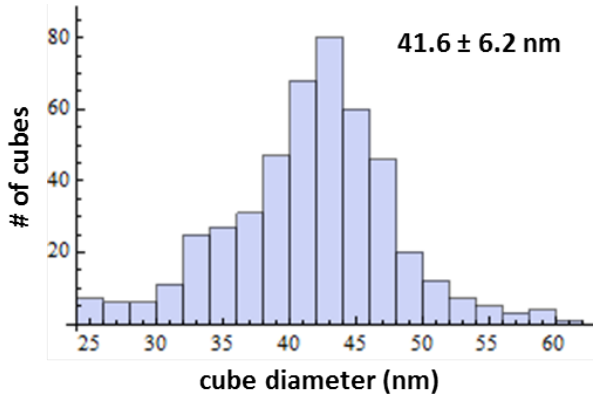

Figure 6: *A histogram of the size distribution of the synthesized silver nanocubes. An imaging program was used to convert an SEM image of cubes to a black and white image, and count and measure the particles. An average cube size of 41.6 nm ± 6.2 nm is calculated.*

2.4 Conclusion

In this section the synthesis of silver nanocubes is shown. A typical synthesis yields, in addition to cubes, wires and large particles. These particles are removed by filtering and centrifugation, leaving cubes with an average size of 41.6 nm (± 6.2 nm). For the realization of a grid the cubes need to be assembled in a rectangular lattice pattern, which is described next.

3 Assembly

3.1 Introduction

This chapter reports on the assembly of silver nanocubes in a rectangular pattern in a textured mold and shows the transfer of these assemblies to a substrate. For assembly, a substrate with nanoscale pattern is immersed vertically in a suspension of nanoparticles and slowly pulled out (see the illustration in figure 7). This dipcoating technique was used by Cui et al. to assemble nanospheres of 50 nm diameter [23] and is shown with cubes here. While patterned SiO_X was used in their work, here assembly is demonstrated in a patterned polydimethylsiloxane (PDMS) substrate. This material is chosen for its flexibility, which permits transfer of the assemblies to another substrate. The fabrication of the PDMS mold requires an original pattern as a template, which is produced using a soft conformal imprint lithography (SCIL) technique [21]. This technique allows for large scale imprinting of nanoscale patterns in resist. Subsequent lift off and evaporation of metal results in the desired patterns. A copper square grid pattern on glass is used here as a template for the PDMS mold (see figure 8). The methods for the PDMS mold fabrication, dipcoating and transfer are described next.

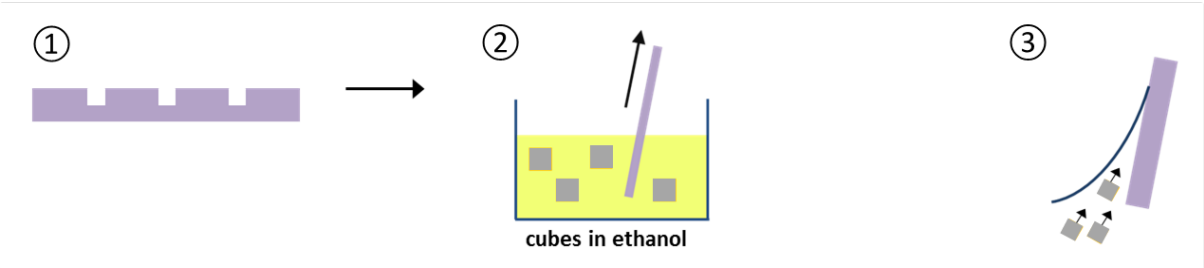

Figure 7: *1) A mold with nanoscale pattern. 2) The mold is immersed in a suspension of nanocubes and slowly pulled out. Through this dipcoating process cubes assemble in the nanoscale pattern. 3) Magnified view of the contact plane. The evaporation of liquid causes a capillary flow of cubes towards the contact plane. Upon slow vertical removal of the mold, cubes are forced into the pattern. This mechanism is described in more detail in the results.*

3.2 Methods

PDMS mold fabrication As a template for the PDMS mold, a chromium nanowire grid on glass was made by Jorik van de Groep following literature [17]. The template consists of several 2x2 mm fields with a pitch varying from 300 to 1000 nm and a wire width varying from 60 to 100 nm. The height of the wires is 80 nm. To use this template as a master for the PDMS mold the glass surface of the template must be hydrophobic in order to prevent PDMS from sticking. The glass surface is exposed to fluorosilane (1H,1H,2H,2H-perfluoro-octyltriethoxysilane, Sigma Aldrich, 667420-5G) vapour in a low pressured environment for 5 hours. After this treatment the hydrophobic nanowire template is sonicated in acetone for 15 minutes to clean.

PDMS is prepared by mixing the pre-polymer and the curing agent in a 10:1 weight ratio (Dow Corning, Sylgard 184 silicone elastomer, LOT: 0007426830). The mixture is left in atmosphere for roughly 20 minutes to degas, after which the PDMS is poured over the template, in a small container, untill a thickness of 5-8 mm is reached. The template

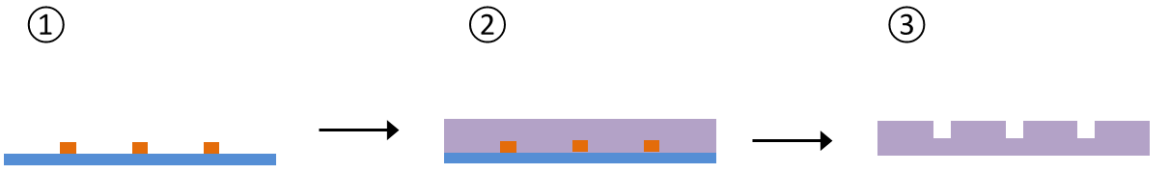

Figure 8: *Schematic image of the fabrication of the PDMS mold. The nanowire network (1) is covered with PDMS (2) and cured in a 100°C oven for 30 minutes, resulting in a PDMS mold with nanotrenches (3).*

needs to rest in atmosphere for 5 minutes to ensure that the PDMS covers all features. The curing agent catalyzes a crosslinking reaction between silicon hydride (-SiH) and vinyl (-CH=CH_2) groups in the pre-polymer, forming a solid yet flexible material. This curing is accelerated by baking the PDMS in a 100°C oven for 30 minutes. After cooling down for several minutes the mold is peeled off of the glass.

Dipcoating The PDMS mold is cut into small pieces (5 x 20 mm) that are cleaned by sonication in acetone for 10 minutes. For the slow retraction of the molds from a liquid a home-built dipcoating setup is used. This setup consists of inverted tweezers attached to a syringe pump (KR analytical, Chemyx Fusion 400 Touch) that can pull at a very slow rate (see figure 9). The PDMS pieces, held by the tweezers, are immersed in a cube suspension vertically and pulled up at a rate of 75 μm min^{-1}. In this experimental setup the cubes are suspended in ethanol. As a measure for the nanocube concentration, the absorbance peak of the suspension was measured. The cube suspension used showed (diluted 600 times) an absorbance peak of 0.014 at 444 nm (optical path 1 cm). This absorbance measurement was done in a UV/VIS/NIR spectrometer (Perkin Elmer, UV/VIS/NIR Spectrometer Lambda

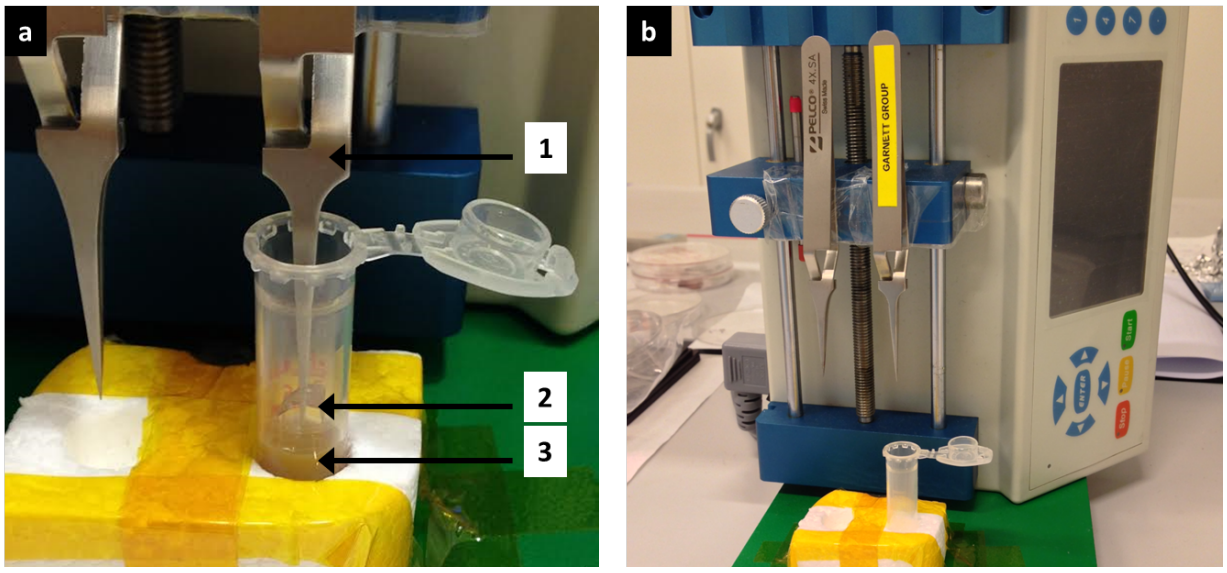

Figure 9: a: *Image of the home-built dipcoating setup. In the back the syringe pump is visible (put on its side to pull in vertical direction).* **1)** *Inverted tweezers holding the PDMS substrate are attached to the pump.* **2)** *A PDMS substrate of 5 x 20 mm.* **3)** *The suspension of silver nanocubes in ethanol, contained in an eppendorf tube.* **b:** *Overview of the setup.*

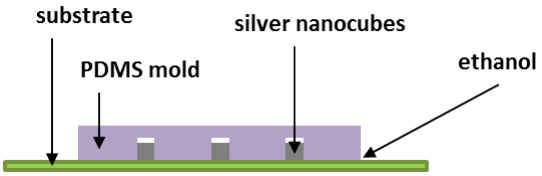

Figure 10: *Schematic image showing the method used to transfer cubes from the PDMS mold to a substrate. The mold is placed on the substrate that was wetted with ethanol, and is then left to dry. After drying the mold is pulled off and cubes are transferred to the substrate.*

750) in an integrating sphere.

Transfer After assembly in the patterned mold through dip-coating, the silver cubes are transferred to another substrate, quickly after the ethanol contact line has crossed all patterns. The mold is placed on top of a substrate which was previously wet by ethanol (see schematic in figure 10). The flexibility of the PDMS ensures proper contact between the mold and the substrate. Without applying force the PDMS mold is left to dry in atmospheric conditions. After half an hour the ethanol has evaporated and the PDMS is peeled off. This process ensures the transfer of cubes to silicon, quartz and a TEM grid (Ted Pella, Ni mesh, carbon based polymer membrane, Lot # 250913 01800N-F). No specific cleaning of the substrates is required.

3.3 Results

Assembly Using the method just described silver nanocubes were assembled in the grid shaped trenches of a PDMS mold across entire 2x2 mm fields. An optical microscope image shows this assembly on a large scale in figure 11a. Figure 11b shows an SEM image of the cubes embedded in the PDMS mold[1]. In several lines the cubes are aligned properly (e.g. at arrow 1). A few deficiencies in the assembly are also apparent in this image.

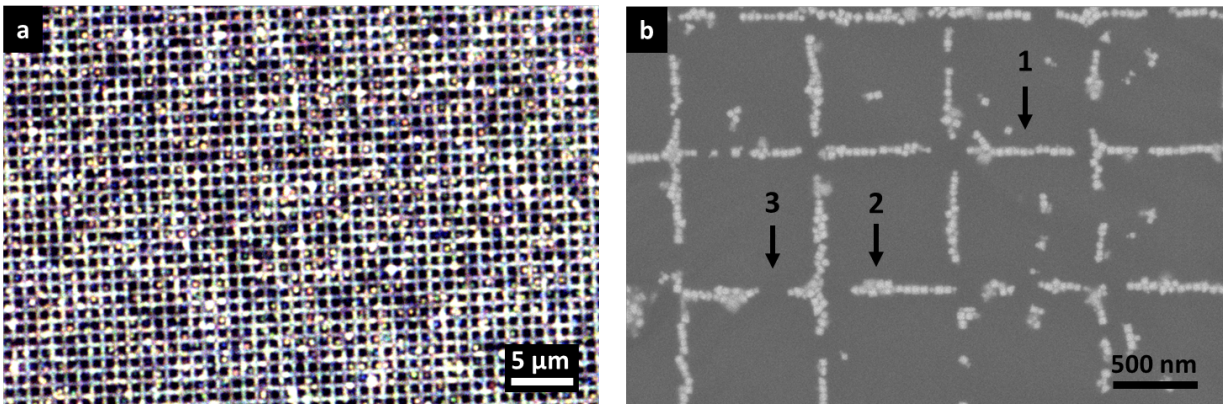

Figure 11: a: *A dark field optical microscope image of silver nanocubes assembled in a PDMS mold.* **b:** *An SEM image of the cubes assembled in a PDMS mold. Arrow 1 denotes a continuous line of cubes. Arrow 2 and 3 mark defects: respectively double assembly and an interruption in the pattern.*

[1]To image the non-conducting PDMS mold in the SEM, the surface needs to be covered with a conductive layer. Here, several nm of chromium is deposited by sputter coating. This, together with drifting of the flexible PDMS during imaging, decreases the resolution of the image.

First, in some lines the cubes form a double row (arrow 2). As the cubes are the building blocks for transparent electrodes, a double row will result in a wider electrode. This will decrease the optical transparency of the final grid. A second defect in the assembly shown in figure 11b is the presence of gaps in the lines (for example at arrow 3). Unconnected electrodes will increase the sheet resistance of the grid. To minimize the sheet resistance of the transparent electrode grid, the filling of the trenches must be improved.

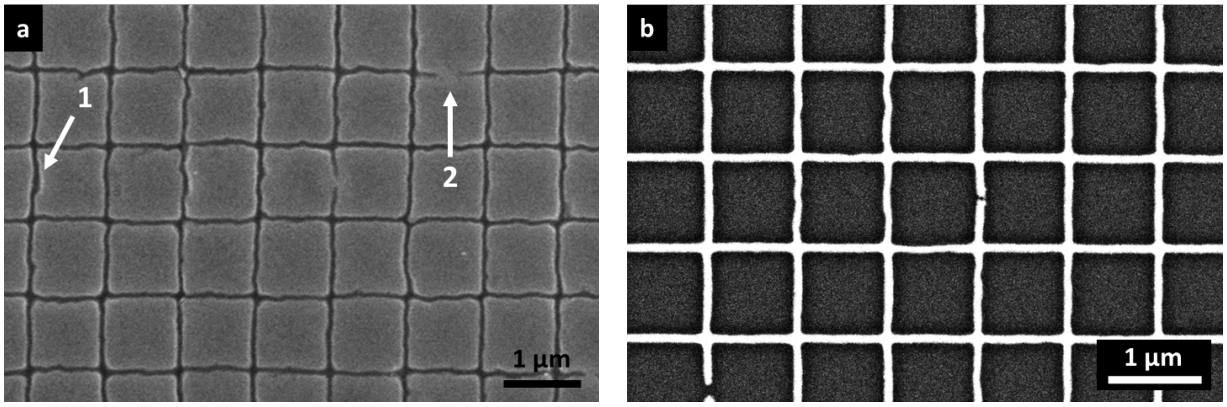

Figure 12: a: *An SEM image of the PDMS mold before dipcoating. Arrow 1 shows local widening of a trench, arrow 2 shows a defect in the mold.* **b:** *An SEM image of the evaporated chromium wires on glass, used as a template for the PDMS mold.*

Factors that influence assembly The assembly defects just mentioned can be caused by a combination of (i) the quality of the trenches in the PDMS mold, (ii) the size dispersion of the cubes and (iii) the dipcoating parameters. The effects of these three factors are discussed here.

To investigate (i) the effect of the trench shape on assembly, the PDMS mold is examined before it is used for dipcoating. Figure 12a shows an SEM image of part of a PDMS mold. The width of the trenches is seen to vary, for example at position 1. This wider trench allows multiple rows of cubes to fit in, as was observed in the assembly (figure 11b). If on the other hand a trench would be too narrow, the assembly of cubes in a single line is also hindered, as cubes do not fit. One might expect to see assembly of the smallest cubes in such a trench, however figure 11 does not show small cubes in a line. It is thus more likely that narrow trenches are not filled. Therefore, the variation of the trench width in the PDMS mold can cause both of the assembly defects observed in figure 11b.

To improve the assembly of cubes (minimizing interruptions and overfilling) a constant trench width in the PDMS mold is required. The width variation likely originates in the chromium wire template, because the trenches in the PDMS mold obtain their shape from this template. If the template contains defects these will be copied to the PDMS mold. An image of the chromium wire template is shown in figure 12 b. The width of the chromium wires is not constant, which explains the width variation in the PDMS trenches (as seen in figure 12 a). The chromium wires, in turn, obtain their outline indirectly from the SCIL stamp: the pattern printed with this stamp was copied to our template by the deposition of chromium. It is possible that this deposition procedure introduced the variance in wire width. This procedure could be fine tuned, however the metal deposition step can be omitted by employing for example etching to fabricate a template. At present, through

the etching of silicon an alternative way to fabricate a wire template is studied, of which preliminary results are shown in the Appendix (figure 31).

Apart from the varying trench width (that was shown to cause interrupted and double-layered assembly), an interrupted trench is seen in the PDMS mold in figure 12a (marked by arrow 2). This interruption will cause a gap in the assembly. Yet, the gaps in the assembly in figure 11b can not be explained solely by these interrupted trenches, as these defects are scarce (see also figure 13). Another cause for the observed gaps in the assembly of cubes is discussed next.

A second factor that unfluences assembly is (ii) the size dispersion of the silver cubes. The cubes fabricated and used in this research show a relatively broad size dispersion, as seen in figure 6 in the previous section. Small cubes might induce double layered assembly, while large cubes are thought to cause interrupted assembly by hindering proper sized cubes.

For a better understanding of how large cubes can cause interrupted assembly, the principle behind nanoparticle assembly by dipcoating is discussed here. This mechanism, leading to the collection of particles in nanoscale features, was examined by Liddle et al. [37]. When a nanopatterned substrate is immersed in a suspension of nanoparticles, the fluid wets the substrate. Because of this wetting the layer of fluid close to the contact plane is thin. Upon evaporation of the fluid this layer becomes thinner, and the surface tension pulls the contact plane down in order to maintain the shape of the fluid surface. However, the patterned features in the substrate induce pinning of the contact plane. A capillary flow of liquid towards this pinned contact plane is necessary to counteract the deformation of the fluid plane. This replenishing flow of liquid pulls nanoparticles along, which accumulate at the pinning site. This evaporation induced accumulation of particles at the edge of a liquid plane was reported by Deegan et al. [38] and is illustrated in daily life by the ring-shaped stains formed by drops of coffee. By pulling the substrate upwards the contact plane is shifted down. This moving contact plane, having a small contact angle with the substrate, pushes particles in the features as the plane moves over the substrate [37].

When our nanocubes assemble at the contactplane, our hypothesis is that they form a monolayer. With the continuous supply of cubes they likely take a close packed 2-D structure. This idea is supported by the fact that (as seen in figure 11b) multiple cubes assemble close together in one line. It is unlikely to obtain this result without the formation

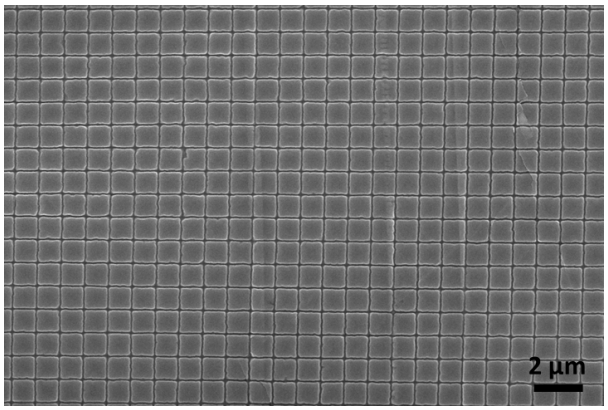

Figure 13: *SEM image of a large region of a PDMS mold with trenches. It shows that nearly all trenches are continuous.*

of a close packed monolayer of cubes. This monolayer configuration, in combination with a broad size dispersion of the particles, is thought to be the reason for gaps in the assembly: if a large cube in the monolayer is pushed in a trench by the fluid plane it will not fit, and it will remain in the liquid. The smaller neighboring cubes on the other hand do fit and the absence of the bigger cube results in a gap in the assembly. As cubes enter a trench only once the fluid plane moves over this trench, a second opportunity for filling a gap is not there. In conclusion: it is our belief that the assembled lines of cubes will be less interrupted when a monodisperse cube suspension is used.

The formation of a 2-D monolayer of cubes prior to assembly in trenches can also explain why assembled lines consisting of small cubes are not observed (which was noted before): for this to happen a line of only small cubes must be formed already in the monolayer, which is unlikely statistically.

The PDMS trench quality and the size dispersion of the cubes have been discussed as possible causes for imperfect assembly. Lastly (iii), assembly may be influenced by the parameters for the dipcoating procedure. It was reported that the nanoparticle concentration, the pulling speed and the contact angle between fluid and substrate all influence assembly [23]. The first two parameters were optimized for our assembly and are discussed next.

The effect of nanoparticle concentration on assembly is generally recognised [39–41]. The concentration of our nanocube suspension is found to be important too. Dipcoating experiments were performed using a range of nanoparticle concentrations. At high concentration the nanocubes overfilled the trenches. Cubes additionally aggregated on the PDMS surface in between the trenches. This is probably induced by the overfilled trenches, forming embossed features that allow accumulation. On the other hand, at low concentration the trenches were sparsely filled. At the optimal concentration most lines looked continuous in the optical microscope, while (although just resolved in the microscope) the surface between the assembled lines seemed mostly free of particles.

As representation for the concentration of the cubes the absorbance spectrum of the suspension is used. A peak in this spectrum represents the nanocubes having a plasmon resonance at a specific wavelength, at which the particles absorb maximally. The concen-

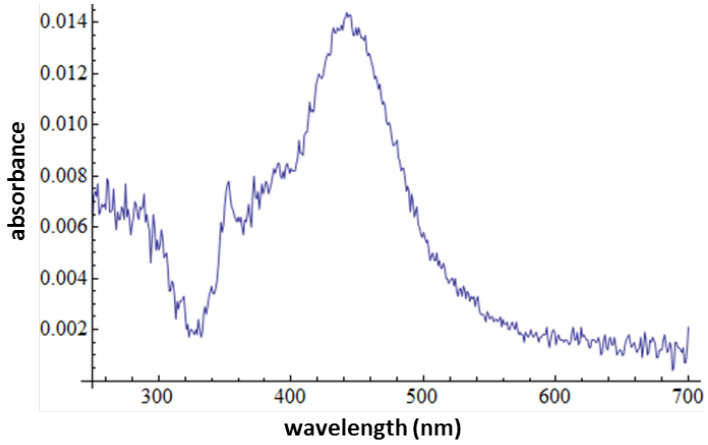

Figure 14: *An absorbance spectrum taken from the suspension in which assembly was found optimal. The absorbance peak is 0.014 at 444 nm. The measurement was done on a 600 times diluted sample in the integrating sphere of a UV/VIS/NIR spectrometer.*

tration of particles scales linear with the absorbance peak. At the concentration optimal for assembly the absorbance spectrum of the cube suspension was measured in a UV/VIS/NIR spectrometer as decribed in the methods (note that the suspension was diluted 600 times for the measurement). This spectrum is shown in figure 14. At 444 nm the absorbance peaks at a value of 0.014. Assembly was also achieved using suspensions of slightly higher and lower concentrations. For these suspensions absorbance values of 0.020 and 0.005 were measured.

The second parameter that was optimized for dipcoating is the pulling rate. For the assembly of the silver nanocubes a pulling rate of 38 μm min^{-1} was initiated. This resulted in cubes both inside and outside the trenches. To assemble particles primarily inside the trenches the pulling rate was doubled, resulting in assembly as shown in figure 11b.

The final parameter reported to influence assembly is the contact angle between solvent and substrate. The ideal angle reported is 10 - 30 degrees [23]. Here, the contact angle has not been a topic of research. Ethanol is seen to wet our patterned PDMS substrate strongly, the contact angle is very probably in the 10 - 30 degree range.

It should be remarked that since both concentration and pulling speed are already optimized, and the contact angle corresponds with literature values, little improvement in assembly is foreseen by fine tuning these parameters. Better assembly is expected mainly by improving the trench shape in the PDMS substrate and, more importantly, narrowing the size distribution of the cubes. Only once these parameters are addressed, the dipcoating parameters can be studied further.

Transfer After the silver nanocubes have been assembled in trenches in the PDMS mold, they are transferred to another substrate. With the procedure described in the Methods, the assemblies were transferred from the mold to silicon, a TEM grid and quartz (figures 15a, 15b and 15c respectively). In general, the transfer shows neatly aligned cubes: transfer does not seem to disturb the alignment. On a large scale, transfer is seen to be partially succesful: cubes at the edges of the (5 mm wide) PDMS mold are generally transferred,

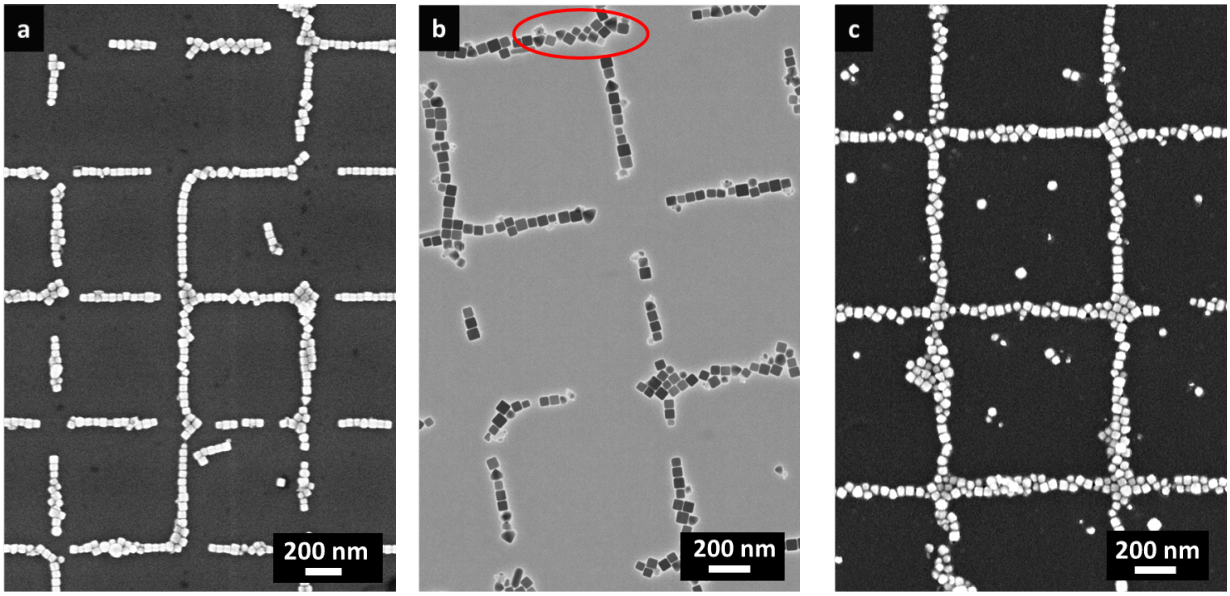

Figure 15: *SEM images showing the transfer of silver nanocubes to different substrates: silicon, TEM grid and quartz (***a***,* **b** *and* **c***).* **b:** *Image taken in transmission mode. The marked region shows small and triangular shaped particles hindering the assembly.*

whereas the cubes in the center of the mold are not. To determine whether all cubes at the sides of the mold had transferred, the mold was examined in the optical microscope, which revealed that a few particles were left in the mold. This explains some of the gaps in the assembly shown in figure 15, but the majority of these gaps must be caused by defects in the initial assembly of cubes.

It is likely that the transfer of particles depends on the wettability contrast between the hydrophilic substrate and the hydrophobic mold. This is also observed by Hamon et al. [41]. The mechanism behind the transfer is not fully understood, but expected to be as follows. Given that cubes are barely present outside the trenches in the PDMS mold after assembly (see figure 11b), the interaction between PDMS and cubes seems to be poor. Cubes interact more strongly with ethanol, such that the ethanol film on the substrate and the ethanol film remaining around the assembled cubes can merge, as soon as the PDMS-ethanol-substrate interface is formed. Since the substrate is more hydrophilic than PDMS, the evaporation of ethanol will be initiated at the PDMS surface. In the temporary PDMS-air-ethanol-substrate interface the cubes will be suspended in ethanol. The surface tension of the ethanol may induce migration of the cubes out of the trenches, by exerting a pulling force during further evaporation of the liquid. As soon as the silver cubes touch the substrate the Van der Waals forces are dominant and the cubes are transferred.

To test whether the ethanol film on the cubes plays a role in the transfer, the PDMS molds with assembled cubes were left in atmosphere to fully dry prior to transfer. Next, the same transfer procedure was performed. In this case cubes were not printed on the substrate. This observation supports the idea that our transfer method depends on the presence of a thin film of ethanol between PDMS and cube. Hereby is assumed that, at nanometer length scales, the ethanol from the wetted surface is not able to wet a dry cube captured in a PDMS trench.

The image of cubes transferred to quartz (figure 15b) underlines the importance for assembly of using a suspension that is monodisperse in size: the circled area shows how small particles hinder linear arrangement. Furthermore it can be remarked that non cubic particles like triangles disturb linear arrangement. This is seen in the same marked area in figure 15 where triangles break the symmetry of a line.

So far, the cross sectional shape of the trenches in the PDMS mold has not been men-

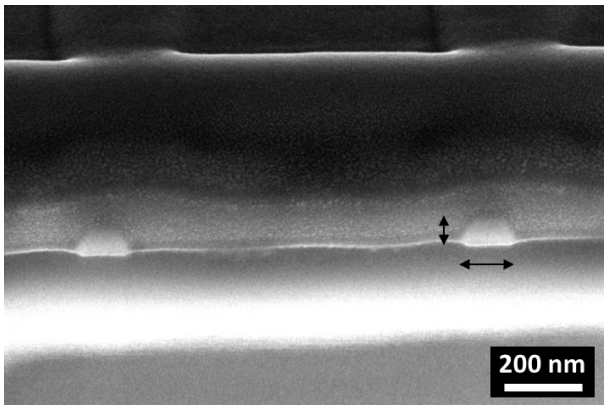

Figure 16: *A FIB cross section of the chromium wires on glass, the template for the PDMS mold. The wires have a slightly rounded shape with dimensions 85 x 130 nm.*

tioned. However, this shape could have an effect on both assembly and transfer. A detailed characterization of the trench and the orientation of an embedded cube would involve performing a cross section of the PDMS mold containing assembled cubes, but this is not yet done. Instead, figure 16 shows a cross section of the chromium wires that are used as a template for the mold. This cross cut was made using a focussed ion beam. The image shows that the height of the wires corresponds with the grid design (85 nm), however the width is larger than aimed (130 nm in stead of 70 nm). Based on the assembly seen earlier (in figure 11 and 15) this width does not seem to cause a problem. The cross section image shows furthermore that the wire contour is not reactangular but slightly rounded. The question is whether a more rectangular trench would improve assembly, although this may complicate the transfer process since in this geometry cubes will be more confined. As mentioned previously, the etching of a wire grid in silicon is currently under study. The preliminary results (shown in figure 31 in the Appendix) indicate that these wires have a more rectangular shape. Once a PDMS mold is made from this new template the effect of a more rectangular trench cross section on assembly and transfer can be determined.

As a final remark, figures 11b and 15 illustrate that nanocube assembly is problematic at the crossings of the grid pattern. Continuous assembly of cubes may be facilitated if a pattern consisting of only parallel trenches is employed. After welding, a grid pattern could then be fabricated from these electrodes by printing vertical wires on top of horizontal wires.

3.4 Conclusion

This section showed assembly of silver nanocubes in a rectangular pattern on a large scale using a relatively simple dipcoating method. Nanopatterned PDMS was immersed in a nanocube suspension in ethanol. Upon slow vertical removal of the PDMS substrate, the trenches were filled with the particles. Several means to improve the quality of the assemblies have been discussed, among which realizing substrate trenches with less variation in width and increasing the monodispersity and shape uniformity of the silver nanocubes. The latter is expected to significantly improve nanocube assembly, since the size dispersion in the cubes used here is relatively large. Lastly, the printing of the assemblies to silicon, a TEM grid and quartz via an easy transfer method is demonstrated. The next section presents several approaches taken to weld neighboring cubes.

4 Welding

4.1 Introduction

The aim of our research is the realization of silver nanostructures with optimal conductivity, hence an electrical connection between the assembled cubes must be established. In other words, a connection with a minimal number of grain boundaries in which conductivity is maximized. After assembly, a small gap between two silver cubes is present, due to a residual PVP layer on the cubes resulting from the synthesis. This gap must be filled with silver atoms in order to obtain a continuous metal structure. The crystal planes of two neighboring cubes are lattice matched. If silver atoms attach to the cubes epitaxially, maintaining a single crystalline structure across this gap should in principle be possible. To develop a suitable strategy for the welding of silver cubes two different welding mechanisms have been investigated here: optical and chemical welding. The optical approach has been attempted because welding has been demonstrated previously with silver wires [42]. The chemical approach allows for a more controllable welding. Both approaches are discussed here.

4.2 Optical welding

The optical welding approach is used to rearrange (surface) atoms and is based on the plasmonic behavior of silver nanoparticles. These nanoparticles support collective oscillations of their free electrons (plasmons) upon excitation at their resonance frequency. If two nanoparticles are in close vicinity their plasmonic modes hybridize to form new collective modes at shifted frequencies [43]. The electromagnetic (EM) field induced by the plasmon resonances can be enhanced very strongly locally, depending on the geometry of the nanoparticles and the distances between them [5]. This enhancement is strong enough to heat the surroundings, which causes surface atoms to migrate. As the system wants to minimize its (surface) free energy, it is energetically favourable for two cubes to merge into one bar. Therefore, the migrating surface atoms will be prompted to fill the gap between cubes.

Plasmonic welding of nanostructures is possible in multiple ways, for example using laser light [44–46]. Broadband illumination was used by Garnett et al. for welding silver nanowires [42]. So far, welding with the objective of epitaxially connecting single-crystalline subunits has not been reported. Here, plasmonic welding using a laser and a broadband lightsource were investigated.

4.2.1 532 nm laser

To make use of a laser for plasmonic welding of two silver nanocubes, the resonance frequency of the dimer must be known. At this resonance frequency the strongest field enhancement occurs, at which welding is possible. To determine the resonance frequency of two neighboring silver nanocubes, the EM field distribution was modelled (by Beniamino Sciacca). In this model two 50 nm edge cubes spaced 2 nm were excited with a 532 nm linearly polarized plane wave. Figure 17a shows the field enhancement in the gap of the dimer at 510 nm. The cubes show a resonance peak at 506 nm, as shown in figure 17b. From this simulation it follows that 506 nm is the optimal pump frequency to excite the resonance in two cubes, if the spacing is 2 nm. For 1 nm spacing the resonance frequency

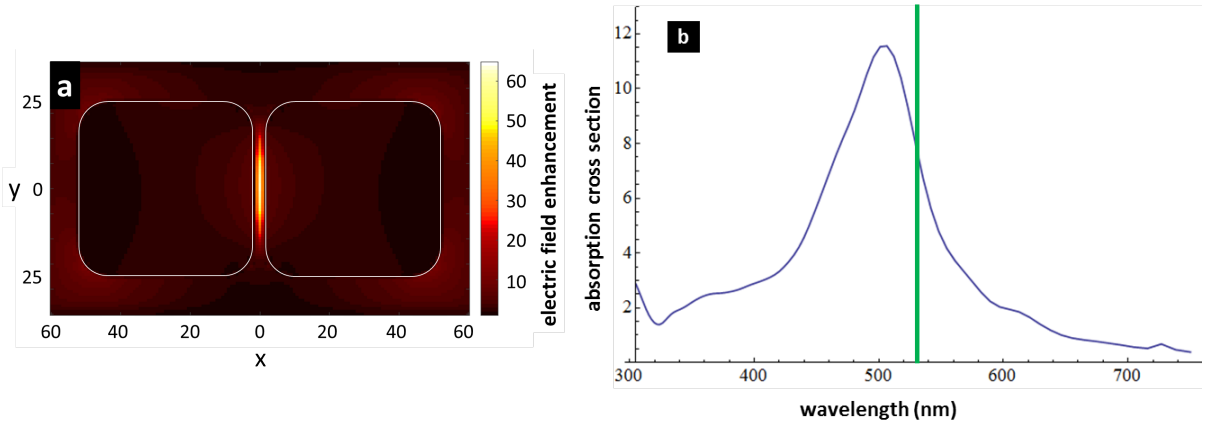

Figure 17: *Simulations of the electric field enhancement and absorption cross section of a silver nanocube dimer excited with a linearly polarized plane wave. The excitation wavelength is 532 nm, the polarization is along the axis of the dimer (the x-direction in* **a***). The 50 nm cubes are spaced 2 nm.* **a:** *Electric field enhancement of the dimer at 510 nm, normalized to the incoming wave. A strong field enhancement is visible in the gap between the cubes. Thin white lines define the edges of the cubes for clarity.* **b:** *Plot of the absorption cross section of the dimer as a function of wavelength. An absorption peak appears at 506 nm. A green vertical line corresponds to the laser wavelength used here for plasmonic welding of nanocubes (532 nm).*

shifts to 518 nm. Using a laser with a wavelength around 515 nm would be optimal for welding 50 nm cubes, assuming that cubes are spaced between 1 and 2 nm. Without this laser at hand a 532 nm laser will be employed. Figure 17 shows a vertical line plotted at this wavelength, showing that at this wavelength the field enhancement of two 50 nm cubes, spaced 2 nm, is 68% of the peak resonance.

Methods A 532 nm linearly polarized laser is used to illuminate aligned silver nanocubes on a silicon substrate. The beam is focussed on the sample through the 100x objective of a microscope (WiTec alpha300), resulting in a spotsize less than 1 micrometer. The dwell time is varied between 0.5 and 2 seconds. The maximum power density of the 100x focussed laser is 401 mW/μm^2, however 43.6 mW/μm^2 is used here. Lines of cubes are excited by scanning the laser over the sample. The area to be exposed is imaged using a CCD camera, in order to position the laser on the line. As diffraction limits the resolution of the image, the 800 nm spaced lines were difficult to differentiate. This hindered the exact positioning of the laserbeam on a line. As the laser spot is a Gaussian, precisely determining the laser power in each exposed line was not possible.

Results Figure 18 shows the result of exposing aligned silver nanocubes on silicon to laser radiation, using a power density of 43.6 mW/μm^2 and a dwell time of 2 s). Figure 18a shows the cubes before illumination, while panels b and c show the changes visible after illumination. With the secondary electron detector it is difficult to image the interfacial welding, as secondary electrons give information mainly about surface topology (see e.g. figure 18 position 3a). Therefore, backscattered electron images are taken as well. Since backscattered electrons are more sensitive to material contrast, welding is more clearly visible in these images (see e.g. figure 18 position 3b).

Figure 18 is representative of several results. It seems that the laser radiation has induced welding as well as melting of cubes. Position 1 shows two cubes that have welded

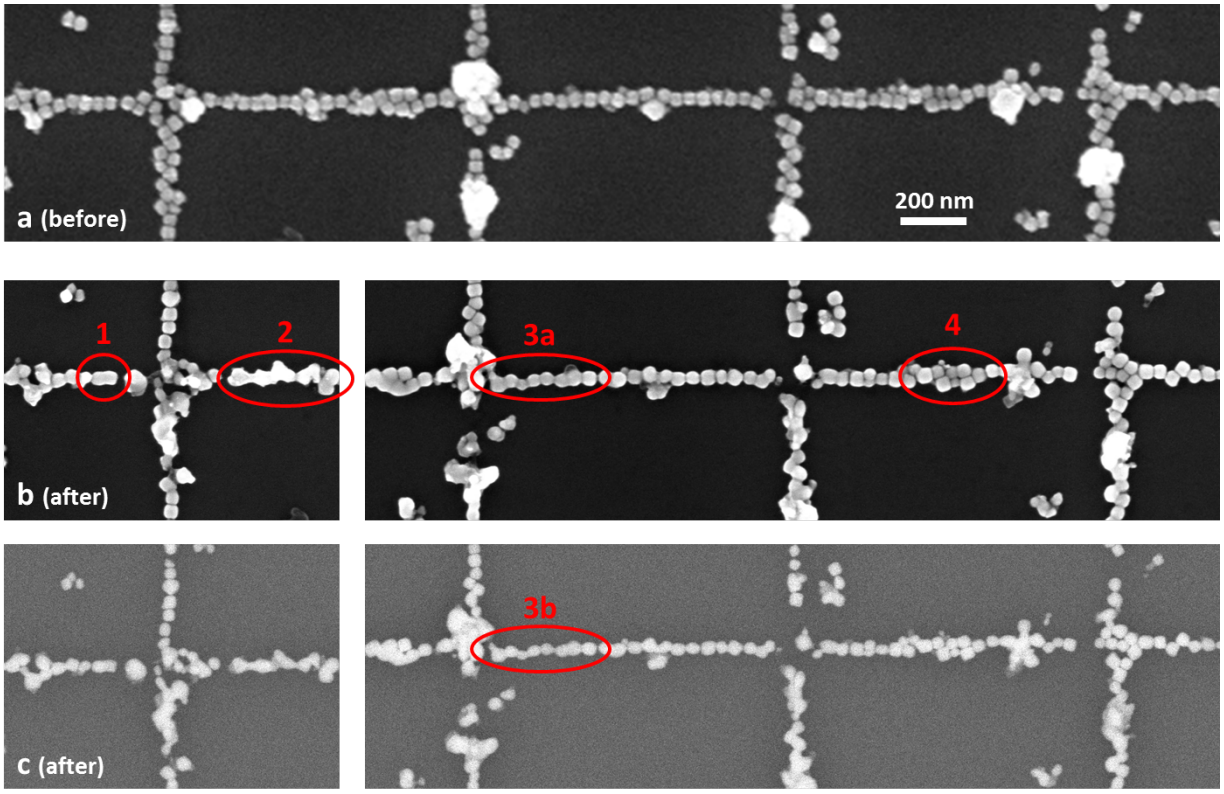

Figure 18: a: *SEM image of aligned silver cubes on silicon, before laser beam exposure.* **b, c:** *SEM images of the same sample after laser beam exposure (532 nm, horizontally polarized, power density: 43.6 mW/μm^2, dwell time: 2 s,* **b:** *detecting secondary electrons and* **c:** *detecting backscattered electrons. The welding of two cubes is visible in position 1, welding of multiple cubes is visible in position 2 (but linear arrangement is lost) and position 3. In the region marked with number 4 the cubes have not welded, possibly due to being in the tail of the laser beam, where the power is too low.*

by means of the laser. Indicated by number 2 are cubes that have probably melted, as their linear arrangement is lost. Furthermore it is observed that at position 4 cubes have not been welded. It is difficult to align the sample with the laser, hence in this sample the scanning trajectory was not perfectly in line with the assembly. As a result, different powers were given to the sample, explaining the welding differences along the line of cubes. To resolve this issue one could use a lower magnification and increase the laser power. When, during a dose test, excess power was used (395 mW/μm^2, dwell time: 1.5 s), the silver melts and forms a ball to decrease its surface area. An example of this is shown in figure 19.

This experiment shows that welding nanoparticles using laser radiation is possible, but it is not very controlled yet. As mentioned, a problem is the limited control over the exact position of the laser and hence the intensity of the beam in a specific spot. Secondly, once two cubes are welded into a bar its resonance frequency shifts [47]. Consequently, the resonance of this bar and the next cube does not correspond with the laser frequency anymore. If the mismatch in resonance between the dimer and the laser is too large, welding in a line is not possible. To quantify this mismatch the resonance frequency of a bar-cube dimer was modelled (results are not shown here). This showed a resonance of 625 nm such that plasmonic welding of a bar and a cube is not possible with a 532 nm

laser. This issue is an intrinsic obstacle in using a monochromatic light source for welding strings of particles. Lastly, as a practical problem, for large scale application laser welding would demand too much time.

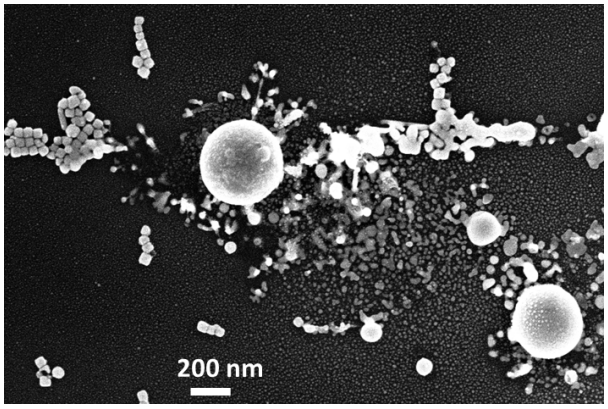

Figure 19: *Illuminating silver nanocubes using laserlight with too much power (395 $mW/\mu m^2$, dwell time: 1.5 s) results in melting and the formation of balls.*

4.2.2 Broadband light

One of the problems occuring upon laser welding is the fact that the resonance frequency of the cube dimer shifts as soon as the cubes have welded. To avoid this issue, a broad spectrum source has been assessed to optically excite a larger range of resonances in assembled silver nanocubes. A Rapid Thermal Anneal (RTA, SITESA Addax) is used as the source. The RTA uses 14 tungsten halogen lamps with a total power of 80 kW for illumination and is originally designed for rapid heating and cooling via optical absorption. The device is temperature controlled via a pyrometer, however only for temperatures above 600°C. For the desired plasmonic effects, here the RTA is used chiefly because of its broadband illumination feature. Since illumination times are chosen such that the melting temperature for nanoscale silver is not exceeded (350°C [48]) the temperature of the particles could not be tracked.

Methods A sample with assembled cubes on silicon is placed on the silicon support wafer in the RTA. Argon flows for one minute prior to and after illumination, and during illumination (5 L/min). Illuminations times of 3 to 6 seconds are tested. Each cycle is completed with a 2 minute nitrogen purge.

Results Figure 20 shows aligned silver nanocubes on silicon before (a-d) and after (e-h) illumination in the RTA. Four samples were exposed for 3 to 6 seconds. For 3 seconds of illumination hardly any changes in the sample are visible (a and e). After 4 seconds (b and f) rounding of the particles occurs, which is seen most clearly for a rod shaped-particle (circled in the images) which has decreased its surface to volume ratio. The same is seen to occur in the cubes, which take a spherical shape. This rounding effect is more pronounced after 5 seconds of illumination (c and g). Illuminating for 6 seconds shows drastic shape change of a wire (d and h). Also the fusion of two cubes in a edge-edge fashion is observed. It should be noted that alteration of the morphology of the particles

does not imply loss of crystal structure. The spheres visible in e.g figure 20f are likely still single-crystal. Shape modification comes predominantly from the surface atoms that rearrange upon illumination, in order to minimize the surface free energy.

Although the morphological changes in the particles (observed in figure 20) indicate that surface atoms are migrating, these atoms remain on the same cube, leaving the particles unconnected. This is confirmed by taking backscattered electron images, not shown here. The fusion of particles might be prevented by the thin layer of PVP on the cubes, residual from the synthesis. Despite the fact that silver diffuses through PVP, this layer might lower the interaction between two silver planes. It is noted that exposing the particles to light for a longer period might increase the chance of welding, however, eventually the silver will melt. Better fusion is therefore expected primarily if the capping layer is removed prior to exposure to broadband illumination. This is easily done thermally or chemically.

Figure 21 shows another part of the sample that was shown in figure 20g (illuminated for 5 seconds). This part of the sample shows more welding events than seen in figure 20. As this part of the sample (figure 21) was not imaged before illumination, it is difficult do determine whether a fusion consists of cubes or other particles, and whether edges or faces have been fused. In two cases (circled) most likely cubes have fused face to face.

The welding in figure 21 might seem randomly distributed: in multiple places cubes have welded, but several other sites remain where cubes are in close contact but still unconnected. However, a closer look at the welding events suggests that welding occurs mainly at crossings in the grid or in a place where more than two particles are together. Hotspots in silver nanocubes are stronger at the edges than at the faces. At the crossings of the grid pattern the chances that cubes orient edge-face or edge-edge is higher than between crossings, where cubes align face-face. This may explain the more frequent welding of clustered cubes, as compared to the less frequent face-face welding.

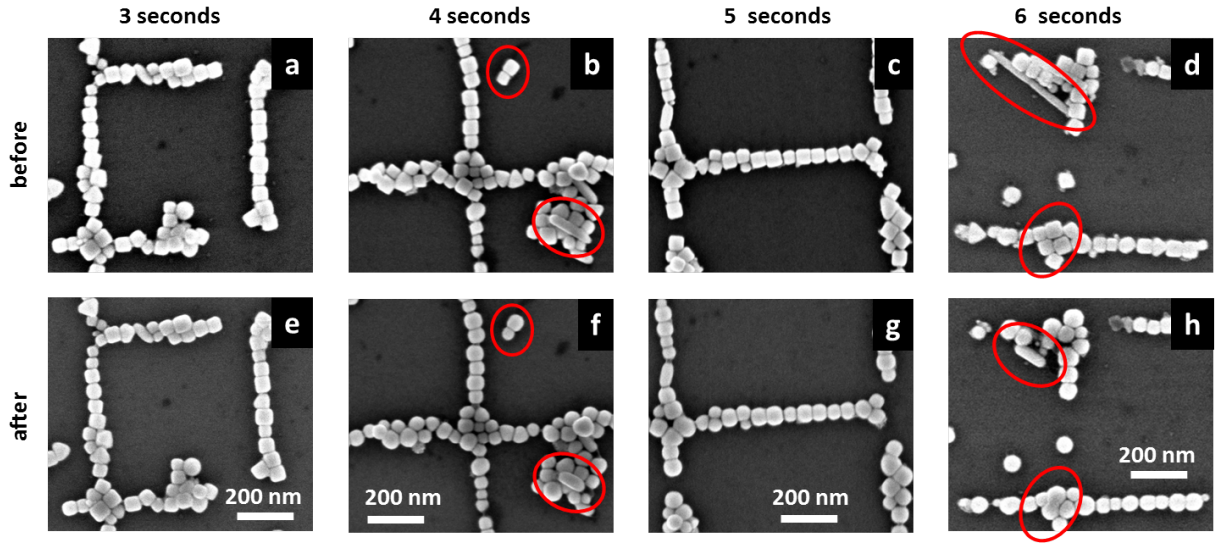

Figure 20: *This image shows silver nanocubes on silicon before* **a-d** *and after* **e-h** *illumination with a broadband light source for 3 to 6 seconds. After 3 seconds the particles have not changed much. After 4 seconds the surface to volume ratio of the particles is decreasing. This is visible by rounding of cubes and shrinking of a wire. After 5 seconds these effects are more pronounced. After 6 seconds a wire has shortened to a fourth of its length, and two cubes have fused at their corners. These images do not capture many welding events (see figure 21 for more welding events after 5 seconds), but they do illustrate the effect of broadband light for increasing exposure time.*

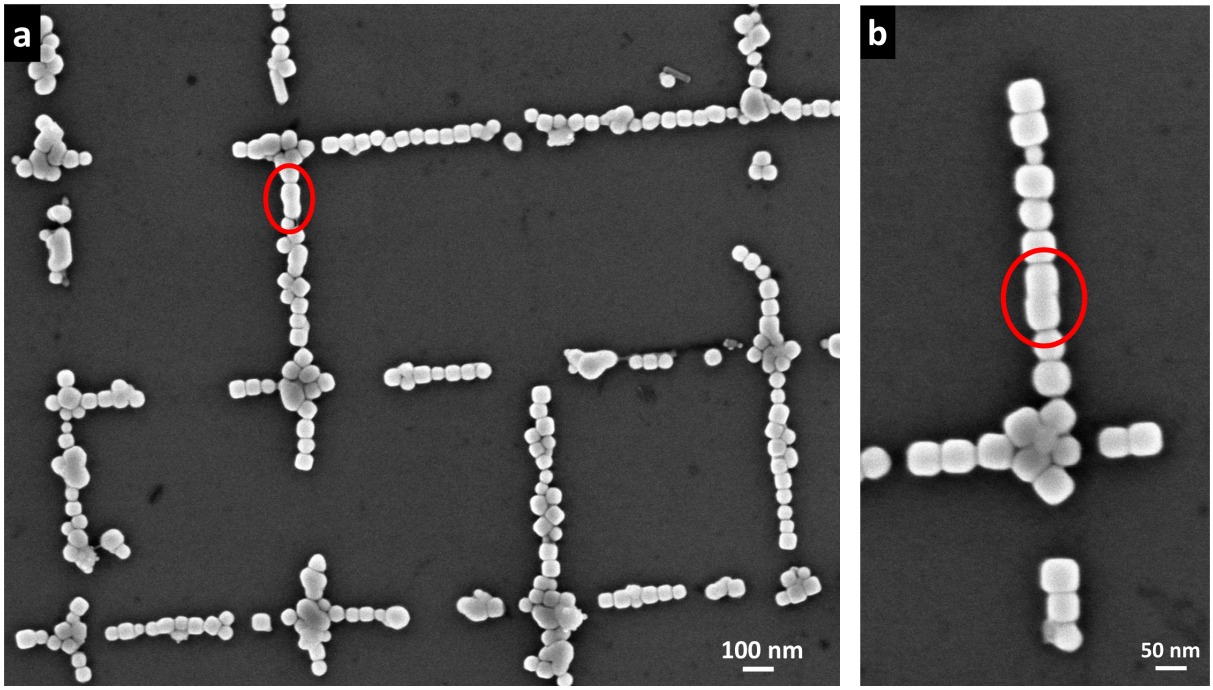

Figure 21: *SEM images of welding events in silver nanocubes aligned on silicon. The particles were illuminated for 5 seconds with a broadband light source.* **a:** *This part of the sample shows many fusions. The welding in the marked region seems to originate from two face to face cubes, but for other welding events it is not possible to determine how the cubes were oriented prior to welding.* **b:** *Another part of the same sample in which two cubes have welded face to face (circled).*

4.3 Chemical welding

The second approach for welding silver nanocubes that was examined here relies on chemical reactions to add or rearrange silver atoms. In a first experiment adding silver is demonstrated using Tollens' reagent. The reaction involves the reduction of a silver precursor to elemental silver, which nucleates on and in between the silver cubes. In a second experiment silver nanocubes are welded using the reducing agent $NaBH_4$. In this experiment no new silver is added, but the surface atoms of the silver cubes are rearranged such that particles can merge. In a final experiment, silver is deposited merely at the interface of neighboring cubes, using Tollens' reagent. Several drops of this reducing agent are applied to cubes on silicon and excess liquid is subsequently removed by blow-drying.

4.3.1 Tollens' reagent

Methods 0.204 g silver nitride ($AgNO_3$, Sigma-Aldrich CAS 7761-88-8) is dissolved in 5 mL d.i. water to obtain a concentration of 0.24 M. 10 μL of a 0.25 M potassium hydroxide (KOH, Sigma-Aldrich CAS 1310-58-3) solution is added to this. The silver oxide (Ag_2O) formed in this reaction precipitates, giving a brown color. Ammonium hydroxide (NH_4OH, 28 - 30 % in water, Sigma-Aldrich CAS 320145-1L) is added until the mixture becomes transparent, roughly 200 - 300 μL is needed. In this step a diammine silver complex ($[Ag(NH_3)_2]^+$) is formed. This complex can be reduced by glucose. 17.11 g glucose ($C_6H_12O_6$, Sigma CAS 50-99-7) is dissolved in 50 mL d.i. water and 25 mL methanol (CH_3OH, Biosolve CAS 67-56-1).

Silver cubes are dropcast on a silicon substrate and left to dry. 5 mL of the glucose/methanol solution is added to the diammine silver mixture. After quickly mixing on a stirring plate (10 seconds) the silicon samples are immersed in this mixture. This experiment is done with five samples (each in 2 mL of the mixture) for periods of 1, 2, 3, 5 and 10 minutes.

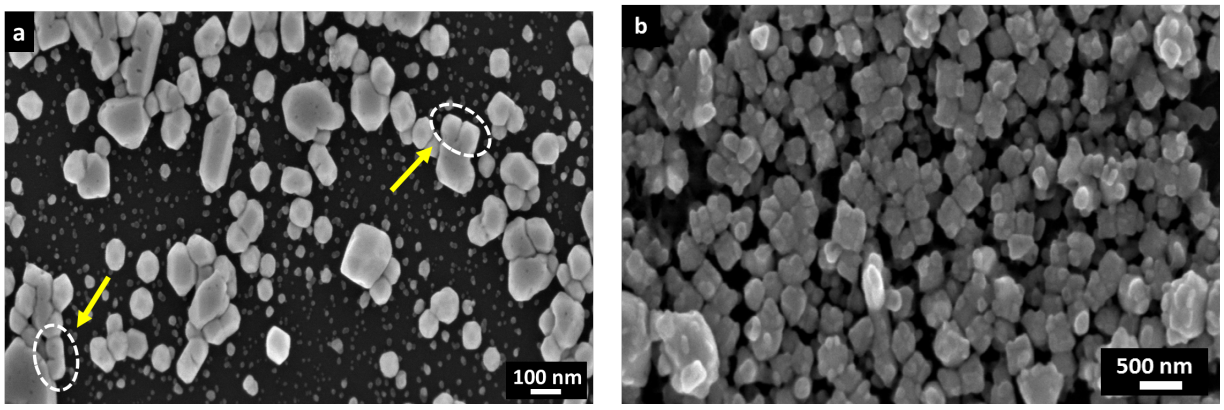

Figure 22: a: *Silver nanocubes on a silicon substrate after being treated with reduced Tollens reagent for 3 minutes. Circled are two positions where cubes have welded face-face. For most other fusions it is not possible to trace the orientation of the cubes.* **b:** *Same sample, this part of the sample was imaged in the electronmicroscope prior to the experiment. The figure shows the deposition of silver on both cubes and silicon. Note that, as compared to* **a**, *the deposited silver takes a grain-like structure here.*

Results Figure 22 shows the result of the immersion of silver cubes on silicon in Tollens' reagent for 3 minutes. This period yielded the best result, as a shorter time did not allow adequate merging, while a longer time integrated all silver cubes into one large structure. To compare the silver cubes before and after the reaction, the sample was imaged in the electron microscope prior to the experiment. After the reaction, the deposition of silver is seen to vary depending on whether a region was pre-exposed to the electron beam or not. These differences in silver deposition are caused by a change in the surface energy of the silicon and the silver. Figure 22b shows a pre-exposed region of the sample. Silver is seen to deposit on the cubes in a grainy fashion. Backscattered electron images confirm welding of the particles (images not included). Apart from adhesion to the cubes, silver is adhered to the silicon substrate. On the contrary, figure 22a (imaged only after the reaction) shows barely silver on the silicon. On the cubes, silver has nucleated neatly such that the particles became connected. It even seems that the crystal facets of the cubes are sustained upon the addition of silver, which could indicate epitaxial deposition. As this region was not imaged previously, it is difficult to see how cubes were aligned before the reaction. Only in two spots (circled) definitely face-face fusion has occured (confirmed by detection of backscattered electrons, not shown here).

An interesting remark is that during welding with Tollens' reagent the PVP layer on the cubes does not seem to obstruct fusion.

4.3.2 $NaBH_4$ solution

Initially, a solution of $NaBH_4$ was used to remove the PVP layer from the silver cubes, as a means to more effectively weld cubes in the RTA for example. In literature this solution is

shown to remove PVP from gold nanoparticles [49]: hydride ions that form when $NaBH_4$ is dissolved in water adhere stronger to a gold surface than PVP, such that the polymer layer will be replaced by hydride. The same treatment succeeded on our silver nanoparticles. Interestingly, when the silver cubes were immersed in the solution a second time after exposure to air, welding was discovered. This welding is thought to be the result of the silver surface oxidizing or sulfurizing when exposed to air, only possible after PVP was removed. This silver oxide or silver sulfide could then be reduced by $NaBH_4$, yielding zero valent silver atoms that nucleated on the silver cubes.

Methods 37 mg of sodium borohydrate ($NaBH_4$, Sigma-Aldrich CAS 16940-66-2) is dissolved in 10 mL water to obtain a molarity of 0.1 M. Silver nanocubes are dropcast on silicon and are dried in atmosphere. The samples are put in the $NaBH_4$ solution for 5 minutes, next 30 minutes in air and subsequently 30 minutes in the $NaBH_4$ solution. The samples are rinsed in d.i. water after the reaction and left to dry.

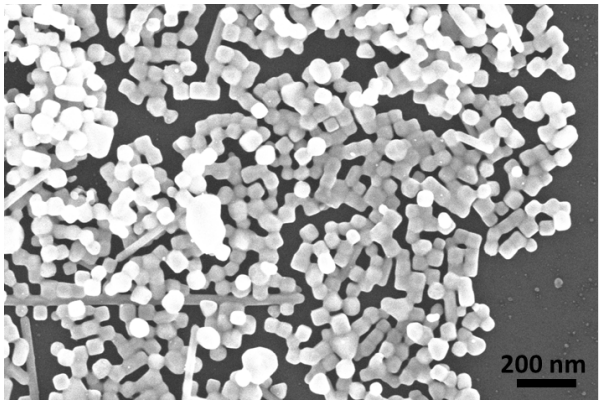

Figure 23: *SEM image of silver nanocubes on silicon, after a chemical welding experiment. The sample was immersed in a 0.1 M $NaBH_4$ solution in water (5 min), left in atmosphere (30 min), followed by a second immersion in a 0.1 M $NaBH_4$ solution in water (30 min). Many particles are connected while the cubic shape of the particles is preserved.*

Results Figure 23 shows magnificent welding of silver nanocubes after the $NaBH_4$ experiment described in the Methods. The shape of the cubes is still clearly visible, and nearly all neighboring cubes are welded. This experiment is repeated several times, and shows very similar results in most cases. Welding is sometimes seen to vary on different regions in the same sample. This is probably the result of contamination of the silicon substrate or differences in residual PVP on the silicon surface after the dropcasting of cubes. The characterization of the silver nanocubes welded using this method is discussed in section 5.

When the intermediate step in atmosphere was skipped (the only reaction being 30 minutes in 0.1 M $NaBH_4$ in water) welding was insignificant. This suggests that a necessary reaction takes place in atmosphere. Our hypothesis is that silver oxide or silver sulfide is formed on the cubes' surface upon exposure to air. Since $NaBH_4$ is a reducing agent it can react with the freshly formed silver oxide/sulfide to form elemental silver. These atoms are then assumed to rearrange across the surface.

4.3.3 Tollens' reagent: local

The mechanism of the $NaBH_4$ induced welding, in particular the effect of exposure to air, is not precisely understood. In addition, this welding procedure takes a relatively long time, as compared to using e.g. Tollens' reagent. Examining the result of Tollens' reagent in figure 22 shows that silver is adhering on all facets of the particles, not only in between. When using $NaBH_4$ on the other hand, the welding is more restricted to the junction (see figure 23), which is preferable. These observations motivated us to apply Tollens' reagent locally, i.e. in between particles. Lu et al. achieved local chemical welding of silver nanowires by immersing a silver nanowire film in a reducing precursor and subsequently blow-drying redundant fluid off the surface [50]. Due to capillary forces of the liquid, a small amount of precursor will remain between the nanowires, which allows reduction of silver ions and the deposition of these zero valent atoms at the nanowire crossings. Here, a similar welding technique is demonstrated for silver nanocubes using Tollens' reagent.

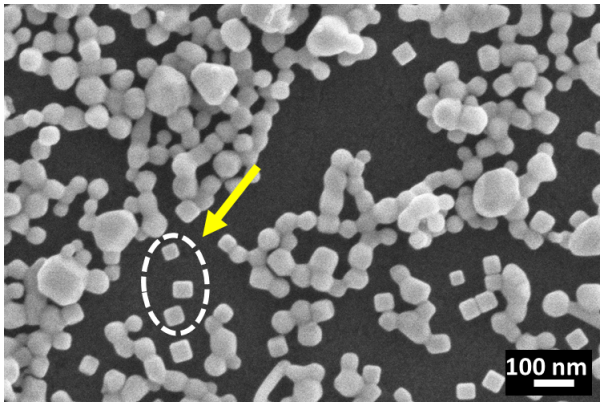

Figure 24: *This figure shows cubes that have welded by applying Tollens' reagent locally. The reagent was dropped on the sample, followed by blow-drying. Through capillary forces the fluid will remain only in the junction between particles. Marked are cubes that are not covered in silver. Since they have no neighbors all reagent was removed by blow-drying.*

Methods Silver nanocubes in ethanol are dropcast on a silicon substrate and left to dry in atmosphere. Tollens' reagent is prepared as described in section 4.3.1. Several drops of this reagent are cast on the substrate with cubes, followed by blow-drying the sample with nitrogen. After 2 minutes in air, allowing silver atoms to deposit on the cubes, the sample is washed in d.i. water and next in IPA.

Results This experiment was performed by Beniamino Sciacca and resulted in welding of cubes as shown in figure 24. As opposed to our previous experiment with Tollens' reagent (figure 22) silver did not adhere to the silicon in this case. Also, the individual particles can still be distinguished, whereas this was more difficult in the previous Tollens' experiment. Both of these observations indicate that the reagent was, as intended, only present between particles that were in close vicinity. This observation is supported by the fact that free standing particles (circled) maintain cubic: no silver was deposited here. By varying the reagent concentration or the reaction time (2 minutes here) the integration of particles is tunable. This experiment shows that control over local welding of randomly oriented nanocubes is feasible, which is very promising for the interconnection of aligned cubes. The easy and quick process additionally permits large-scale application.

4.4 Conclusion

In this section several mechanisms were examined for the welding of silver nanocubes. Optical welding using a laser or a broadband lightsource is relatively uncontrolled, but chemical reactions are shown to be very suited for merging silver particles. Both a reducing solution of $NaBH_4$ in water and locally applied Tollens' reagent show remarkable welding. Characterization of the interface of cubes welded using $NaBH_4$ is demonstrated in the next section.

5 Characterization of interfacial welding

5.1 Introduction

To compare the electric properties of a grid consisting of cubic silver subunits with current TCEs, eventually the conductivity of a line of welded cubes must be measured. Since at present a limited number of cubes has been interconnected, in this section we first investigate the crystallinity of the junction between two cubes. An elegant way to examine the crystallinity of materials is using high resolution transmission electron microscopy (HRTEM). HRTEM makes use of a high voltage (300 kV) electron beam for imaging. Part of the high energy electrons scatter with atoms in a sample, and part of the beam is transmitted. In high resolution mode the phase of the diffracted electron wave is preserved and interferes constructively or destructively with the transmitted electron wave. This technique is called phase-contrast imaging and is used to form images of columns of atoms [51].

5.2 Methods

At this stage of the research transfer of aligned assemblies to a TEM grid was not yet achieved, therefore silver nanocubes (suspended in ethanol) were simply dropcast on the grid (TED Pella, Ni mesh, carbon based polymer membrane, Lot # 250913 01800N-F). Upon evaporation of ethanol the cubes tend to dry face-face to minimize surface energy. This alignment allows for the welding of several cubes. Welding is realized by using a $NaBH_4$ suspension in water as described in section 4.3.2. High resolution images of the samples were taken (by Marijn van Huis) using a FEI/Titan TEM, with a voltage of 300 kV. For characterization of the crystal orientation a fast Fourier transform algorithm in the software ImageJ was used.

5.3 Results

Figure 26b shows a HRTEM image of the junction between two cubes, induced by the $NaBH_4$ reduction reaction. The inset (26a) shows an overview of the cubes. In figure 26b it is first observed that the periodicity of the atoms of both of the cubes is clearly resolved. This is seen in region 1 and region 2. Interestingly, the region within the junction is equally well resolved.

It is important, at this point, to note that high resolution images are affected by focus and specimen thickness in non-intuitive ways [51]. Without a full interpretation of the image shown here (which would involve exactly knowing illumination conditions and objective characteristics) the white 'dots' forming a regular lattice in figure 25b can not be one-to-one designated to be single atom columns. Similarly, the lines (of white 'dots') that are visible are a *representation* of the atomic planes. Still, figure 25 contains much information, for example on crystal structure and orientation.

From the square geometry of the atomic planes it is confirmed that the cubes have a face centered cubic crystal structure. Measuring the periodicity between the planes gives 2.14 Å, which nearly matches the {200} plane spacing.

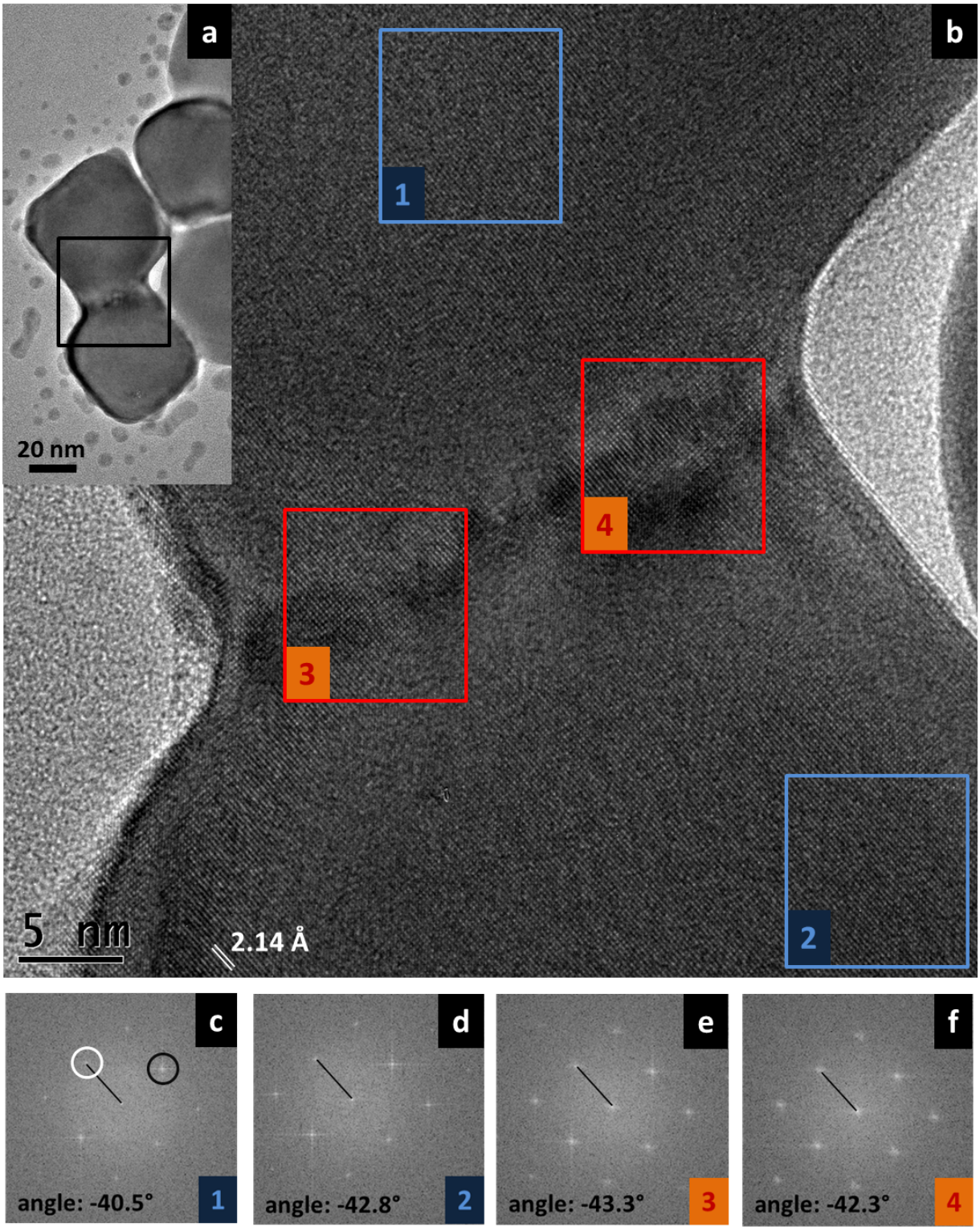

Figure 25: *TEM, HRTEM and FFT images of two silver nanocubes that were chemically welded using a $NaBH_4$ solution.* **a:** *TEM overview. The highlighted area corresponds to* **b.** **b:** *HRTEM image of the junction between the two cubes. In all 4 highlighted regions the atomic planes (a representation therof) are visible. The crystal orientation in these regions is obtained by taking a fast Fourier transformation (FFT).* **c:** *The FFT of region 1. One spot (encircled white) corresponds to crystal planes parallel to the junction, perpendicular planes are represented by the spot that is encircled black.* **d, e, f:** *FFT images of respectively area 2, 3 and 4. The FFT images reveal that the angular spread between all regions is maximally 3 degrees and that the cubes have welded epitaxially.*

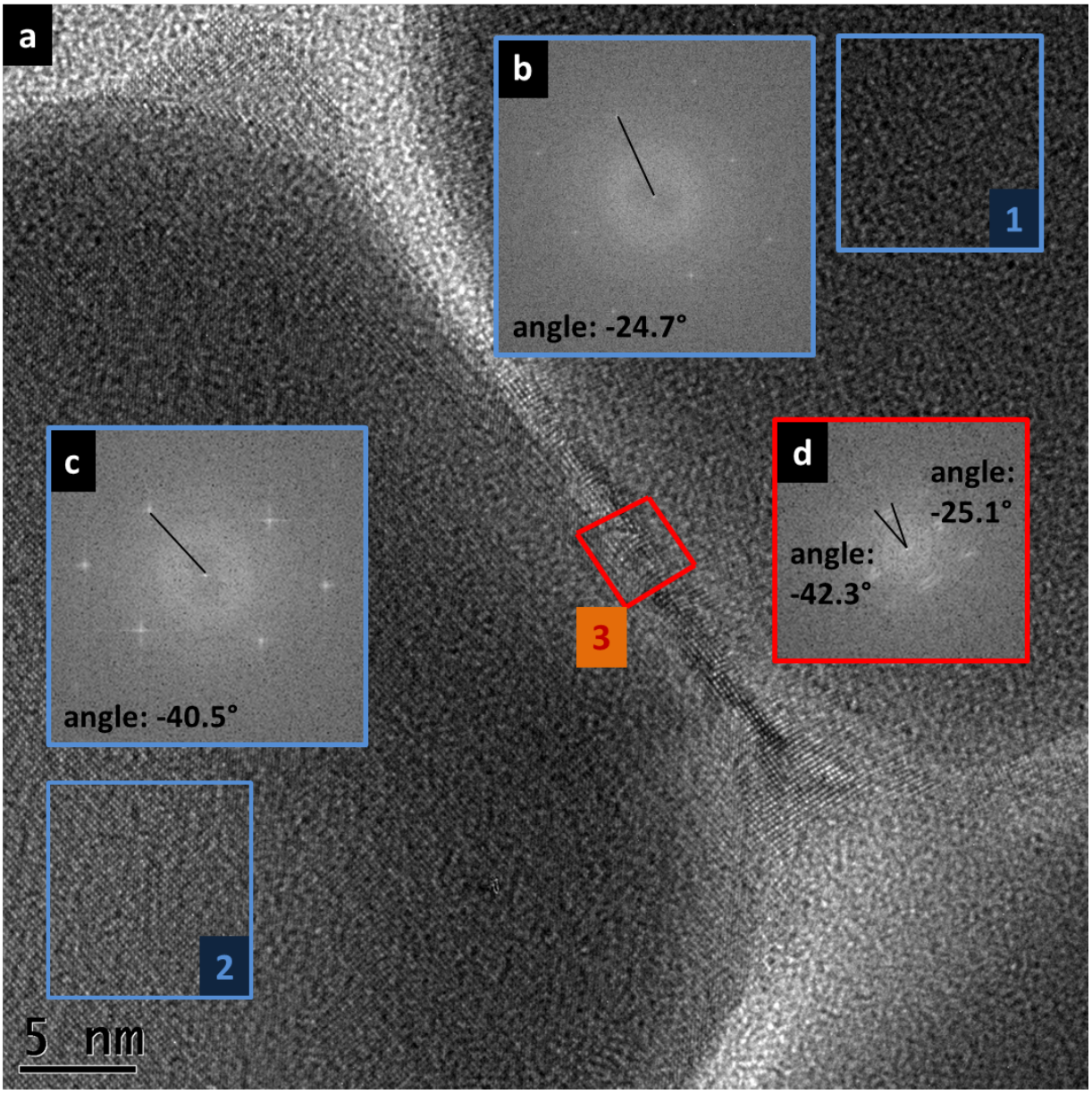

Figure 26: **a:** *HRTEM image of two silver nanocubes that were chemically welded (using a $NaBH_4$ solution). In the junction (e.g. in region 3) the crystal orientation seems to gradually rotate, in order to match the crystal orientations of both cubes.* **b,c:** *FFT images of regions 1 and 2, showing that the two cubes are rotated 15 degrees with respect to each other.* **d:** *FFT image of region 3. The arcs in this image confirm the gradual change in crystal orientation seen in* **a**. *This result demonstrates that even cubes in an angle of 15 degrees can weld epitaxially.*

In region 3 and 4 it is observed that the square periodicity of the lattice is still eminent. This is quite remarkable as the junction is grown by the addition of silver between two silver cubes. To compare the crystal orientation in the gap (regions 3 and 4) with the crystal orientation of the two silver cubes (regions 1 and 2) fast Fourier transform calculations (FFT) were performed on all regions using ImageJ. Figures 25c, d, e and f show FFT images of regions 1 to 4 respectively. An FFT calculation transforms images from real space to frequency space. Periodic lines in real space will be depicted as two single spots (symmetric around the central spot) in Fourier space. In image 25c for example the white marked spot represents real space lines along the cube junction, while the black marked

spot represents lines perpendicular to the junction. This FFT image hence represents a square periodicity in real space, as is observed in region 1. If a spot in an FFT image is sharp, this indicates that the crystal orientation is well defined. This is the case in the FFTs of region 1 and 2 for example.

In figures 25c-f the given angles denote the crystal orientation of the Fourier transformed areas. The two cubes are slightly rotated with respect to each other, which is seen from the difference between the angles in figure 25c and d. The difference in crystal orientation between the cubes is about 2 degrees. Figure 25e and f show the crystal orientation of the region in between the cubes. The dots in these two images are slightly blurred, indicating that the crystal orientation within the junction is less well defined than in the cubes. Still, from comparing all angles it can be concluded that the atoms in the junction are very well aligned with the atoms in the cubes. The largest angular spread (which is between region 1 and 3) is less than 3 degrees.

Optimal conductivity is achieved in crystals with a perfectly periodic atomic configuration. Image 25 shows near-perfect atomic alignment of two cubes with the atoms in their junction: the cubes have welded epitaxially. Therefore our expectation is that the resistance in this dimer is comparable to the resistance in an equally shaped single-crystalline particle.

Figure 26a shows a HRTEM image of two cubes rotated with respected to eachother. The inset FFT images of the two cubes (b and c, taken at region 1 and 2 respectively) show a misalignment of nearly 15 degrees. Note that the spots in figure 25b are weak, caused by a poor resolution in region 1. Although weak, the spots are sharp, and this provides the desired information. When two cubes are misaligned, it is not necessarily expected that chemically added elemental silver will bridge the gap between the particles while preserving the crystal orientation. Fascinatingly, the atomic planes between the cubes seem to be curved, in order to smoothly connect the crystal orientation from one cube to the other. This is visible in various positions along the junction. To qualify this observation, on region 3 an FFT calculation is performed. The result is shown in figure 26d. Instead of spots, the FFT image shows arcs. This indicates that the crystal orientation is not restrained to one angle. Instead, this arc indicates that the crystal orientation gradually shifts along the junction, which is in correspondence with the curving planes in real space that were just mentioned. It appears that the atoms within the junction take position such, that the crystal structure of one cube is connected to the other without interruption. This suggests that the interface prefers a strained epitaxial configuration over grain boundary formation, which holds great promise for conductivity.

5.4 Conclusion

The interface between two chemically welded silver nanocubes was characterized with HRTEM. Analysis of the images through Fourier transformation showed that dimers of cubes had welded epitaxially. This is a very promising result, considering that the silver nanocubes were welded to realise a structure with optimal electric conductivity. Interestingly, the growth of an epitaxial connection is not limited to perfectly face-face aligned cubes. We have additionally shown epitaxial welding for cubes in a 15 degree angle. This enables silver nanocubes to be used as building blocks not only in linear but also in curved geometries.

6 Conclusion

In conclusion, we investigated the feasibility of fabricating single-crystalline silver patterns in an arbitrary shape, by bottom-up assembly and welding of silver nanocubes. As a model pattern, a square grid geometry similar to the nanowire network made by Van de Groep et al. [20] was chosen. In this thesis all parts of the concept are demonstrated to work. The 41 nm $\pm$ 6.3 nm silver cubes, synthesized using a polyol synthesis, were assembled in a flexible PDMS mold on millimeter scale through dipcoating. The pattern was subsequently transferred to different substrates with high fidelity. To establish an electrical connection between the cubes a chemical welding approach involving either Tollens' reagent or a reducing solution of $NaBH_4$ in water is the most promising. With the latter treatment dimers of cubes were welded epitaxially, as is shown with HRTEM. Remarkably, a 15 degree angle between two opposing faces in a dimer yielded, upon welding, a strained epitaxial configuration between the particles. This suggests that in a final structure even curved configurations may be free of grain boundaries.

Now that the concept of single-crystalline patterning is proven, the process can be optimized. The main obstacle in the described procedure is the occurrence of imperfections in the assembly of nanocubes. In this assembly interruptions are assumed to be caused by the size dispersion in the cubes, while local agglomeration of particles is attributed to imperfections in the PDMS trenches. Addressing these issues should lead to better assembly such that a continuous grid can be established. Once such a grid has been realized, performing electrical measurements will allow comparison of this structure with state-of-the-art TCEs.

The results presented in this work open up the possibility of fabricating single-crystalline silver electrode grids, contributing to the research on transparent conductive networks as an alternative for ITO. Moreover, the application of the concept demonstrated here is not limited to silver nanowires: our findings enable the realization of in principle any desired single-crystalline metal structure.

Acknowledgements

My special thanks go to Beniamino, who has shown me the true joy of doing science. Beniamino, I am really grateful for all the days you spent guiding me, answering my questions, being patient, and always staying positive. I enjoyed working with you very much.

Erik, you are a very knowledgeable and inspiring supervisor and it has been a pleasure to be part of your group. I am very glad to have been able to contribute to your 'nanolego' project, and I am curious what future research will bring.

I would like to acknowledge Jorik van de Groep and Marijn van Huis for their contribution to this research. Furthermore, I thank all my groupmembers: Sander, Sarah, Gede, Jia, Parisa, Sebastian, Eric, Linda, Haralds, Jan, Marc, Jenny and Forrest. The discussions and group meetings with you were very educative. Finally, my year would not have been so enjoyable without the new friends I made here.

I am looking forward to seeing you again in January.

References

[1] B. Sciacca, J. Van de Groep, A. Polman, and E. C. Garnett. Solution-grown silver nanowire ordered arrays as transparent electrodes. *Advanced Materials*, accepted for publication November 2015.

[2] D. J. Griffiths. *Introduction to Electrodynamics*. Prentice-Hall, New Jersey, 1999.

[3] Y. Wu, C. Zhang, Y. Zhao, J. Kim, M. Zhang, N. M. Estakhri, X. Liu, G. K. Pribil, A. Alù, C. Shih, and X. Li. Intrinsic optical properties and enhanced plasmonic response of epitaxial silver. *Advanced Materials*, 2014.

[4] A. Rose, T. B. Hoang, F. McGuire, J. J. Mock, C. Ciracì, D. R. Smith, and M. H. Mikkelsen. Control of radiative processes using tunable plasmonic nanopatch antennas. *Nano Letters*, 2014.

[5] S. Mazzucco, N. Geuquet, J. Ye, O. Stéphan, W. Van Roy, P. Van Dorpe, L. Henrard, and M. Kociak. Ultralocal modification of surface plasmons properties in silver nanocubes. *Nano Letters*, 2012.

[6] J. Henzie, S. C. Andrews, X. Y Ling, Z. Li, and P. Yang. Oriented assembly of polyhedral plasmonic nanoparticle clusters. *PNAS*, 2013.

[7] S. Y. Lee, L. Hung, G. S. Lang, J. E. Cornett, and I. D. Mayergoyz ad O. Rabin. Dispersion in the sers enhancement with silver nanocube dimers. *ACS Nano*, 2010.

[8] A. J. Haes and R. P. Van Duyne. A nanoscale optical biosensor: Sensitivity and selectivity of an approach based on the localized surface plasmon resonance spectroscopy of triangular silver nanoparticles. *JACS*, 2002.

[9] A. Tao, F. Kim, C. Hess, J. Goldberger, R. He, Y. Sun, Y. Xia, and P. Yang. Langmuir-blodgett silver nanowire monolayers for molecular sensing using surface-enhanced raman spectroscopy. *Nano Letters*, 2003.

[10] F. S. F. Morgenstern, D. Kabra, S. Massip, T. J. K. Brenner, P. E. Lyons, J. N. Coleman, and R. H. Friend. Ag-nanowire films coated with zno nanoparticles as a transparent electrode for solar cells. *Applied Physics Letters*, 2011.

[11] M. Oh, W. Jin, H. J. Jeong, M. S. Jeong, J. Kang, and H. Kim. Silver nanowire transparent conductive electrodes for high-efficiency iii-nitride light-emitting diodes. *Scientific Reports*, 2015.

[12] K. S. Kim, Y. Zhao, H. Jang, S. Y. Lee, J. M. Kim, K. S. Kim, J. Ahn, P. Kim, J. Choi, and B. H. Hong. Large-scale pattern growth of graphene films for stretchable transparent electrodes. 2009.

[13] X. Wang, L. J. Zhi, and K. Mullen. Transparent, conductive graphene electrodes for dye-sensitized solar cells. *Nano Letters*, 2008.

[14] Z. Yang, T. Chen, R. He, G. Guan, H. Li, L. Qiu, and H. Peng. Aligned carbon nanotube sheets for the electrodes of organic solar cells. *Advanced Materials*, 2011.

[15] K. Lee, Z. Wu, Z. Chen, F. Ren, S. J. Pearton, and A. G. Rinzler. Single wall carbon nanotubes for p-type ohmic contacts to gan light-emitting diodes. *Nano Letters*, 2011.

[16] S. Na, G. Wang, S. Kim, T. Kim, S. Oh, B. Yu, T. Leea, and D. Kim. Evolution of nanomorphology and anisotropic conductivity in solvent-modified pedot: Pss films for polymeric anodes of polymer solar cells. *Journal of Materials Chemistry*, 2009.

[17] J. van de Groep, D. Gupta, M. A. Verschuuren, M. M. Wienk, R. A. J. Janssen, and A. Polman. Large-area soft-imprinted nanowire networks as light trapping transparent conductors. *Scientific Reports*, 2015.

[18] J. Lee, S. T. Connor, Y. Cui, and P. Peumans. Solution-processed metal nanowire mesh transparent electrodes. *Nano Letters*, 2008.

[19] S. De, T. M. Higgins, P. E. Lyons, E. M. Doherty, P. N. Nirmalraj, W. J. Blau, J. J. Boland, and J. N. Coleman. Silver nanowire networks as flexible, transparent, conducting films: Extremely high dc to optical conductivity ratios. *ACS Nano*, 2009.

[20] J. van de Groep, P. Spinelli, and A. Polman. Transparent conducting silver nanowire networks. *Nano Letters*, 2012.

[21] Marc Verschuuren. *Substrate Conformal Imprint Lithography for Nanophotonics*. PhD thesis, Utrecht University, 2010.

[22] Y. Xia, Y. Xiong, B. Lim, and S. E. Skrabalak. Shape-controlled synthesis of metal nanostructures: The case of silver. *Angewandte Chemie*, 2009.

[23] Y. Cui, M. T. Björk, J. A. Liddle, C. Sönnichsen, B. Boussert, and A. P. Alivisatos. Integration of colloidal nanocrystals into lithographically patterned devices. *Nano Letters*, 2004.

[24] B. Gao, G. Arya, and A. R. Tao. Self-orienting nanocubes for the assembly of plasmonic nanojunctions. *Nature Nanotechnology*, 2012.

[25] A. Tao, P. Sinsermsuksakul, and P. Yang. Tunable plasmonic lattices of silver nanocrystals. *Nature Nanotechnology*, 2007.

[26] A. R. Tao, D. P. Ceperley, P. Sinsermsuksakul, A. R. Neureuther, and P. Yang. Self-organized silver nanoparticles for three-dimensional plasmonic crystals. *Nano Letters*, 2008.

[27] J. Henzie, M. Grünwald, A. Widmer-Cooper, P. L. Geissler, and P. Yang. Self-assembly of uniform polyhedral silver nanocrystals into densest packings and exotic superlattices. *Nature Materials*, 2012.

[28] A. R. TAO, J. Huang, and P. Yang. Langmuir-blodgettry of nanocrystals and nanowires. *Accounts of Chemical Research*, 2008.

[29] Q. Zhang, W. Li, L. Wen, J. Chen, and Y. Xia. Facile synthesis of ag nanocubes of 30 to 70 nm in edge length with cf_3cooag as a precursor. *Chemistry a European Yournal*, 2010.

[30] V. K. LaMer and R. H. Dinegar. Theory, production and mechanism of formation of monodispersed hydrosols. *Journal of the American Chemical Society*, 1950.

[31] L. D. Marks. Experimental studies of small particle structures. *Reports on Progress in Physics*, 1994.

[32] B. Wiley, Y. Sun, B. Mayers, and Y. Xia. Shape control of silver nanoparticles. *Chemistry a European Yournal*, 2005.

[33] S. E. Skrabalak, L. Au, X. Li, and Y. Xia. Facile synthesis of ag nanocubes and au nanocages. *Nature Protocols*, 2007.

[34] S. H. Im, Y. T. Lee, B. Wiley, and Y. Xia. Large-scale synthesis of silver nanocubes: The role of hcl in promoting cube perfection and monodispersity. *Angewandte Chemie*, 2005.

[35] A. R. Siekkinen, J. M. McLellan, J. Chen, and Y. Xia. Rapid synthesis of small silver nanocubes by mediating polyol reduction with a trace amount of sodium sulfide or sodium hydrosulfide. *Chemical Physics Letters*, 2006.

[36] B. Wiley, T. Herricks, Y. Sun, and Y. Xia. Polyol synthesis of silver nanoparticles: Use of chloride and oxygen to promote the formation of single-crystal, truncated cubes and tetrahedrons. *Nano Letters*, 2004.

[37] J. A. Liddle, Y. Cui, and A. P. Alivisatos. Lithographically directed self-assembly of nanoctructures. *Journal of Vacuum Science & Technology B*, 2004.

[38] R. D. Deegan, O. Bakajin, T. F. Dupont, G. Huber, S. R. Nagel, and T. A. Witten. Capillary flow as the cause of ring stains from dried liquid drops. *Nature*, 1997.

[39] Z. Quan and J. Fang. Superlattices with non-spherical building blocks. *Nano Today*, 2010.

[40] J. Huang, A. R. Tao, S. Connor, R. He, and P. Yang. A general method for assembling single colloidal particle lines. *NanoLetters*, 2006.

[41] C. Hamon, S. Novikov, L. Scarabelli, L. Basabe-Desmonts, and L. M. Liz-Marzán. Hierarchical self-assembly of gold nanoparticles into patterned plasmonic nanostructures. *ACS Nano*, 2014.

[42] E. C. Garnett, W. Cai, J. J. Cha, F. Mahmood, S. T. Connor, M. G. Christoforo, Y. Cui, M. D. McGehee, and M. L. Brongersma. Self-limited plasmonic welding of silver nanowire junctions. *Nature Materials*, 2012.

[43] N. J. Halas, S. Lal, W. Chang, S. Link, and P. Nordlander. Plasmons in strongly coupled metallic nanostructures. *Chemical Reviews*, 2011.

[44] S. Han, S. Hong, J. Ham, J. Yeo, J. Lee, B. Kang, P. Lee, S. S. Lee, M. Yang, and S. H. Ko. Fast plasmonic laser nanowelding for a cu-nanowire percolation network for flexible transparent conductors and strechable electronics. *Advanced Materials*, 2014.

[45] A. Hu, P. Peng, H. Alarafi, X. Y. Zhang, J. Y. Guo, Y. Zhou, and W. W. Duley. Femtosecond laser welded nanostructures and plasmonic devices. *Journal of Laser Applications*, 2012.

[46] L. O. Herrmann, V. K. Valev, C. Tserkezis, J. S. Barnard, S. Kasera, O. A. Scherman, J. Aizpurua, and J. J. Baumberg. Threading plasmonic nanoparticle strings with light. *Nature Communications*, 2014.

[47] H. Chen, Z. Sun, W. Ni, K. C. Woo, H. Lin, L. Sun, C. Yan, and J. Wang. Plasmon coupling in clusters composed of two-dimensionally ordered gold nanocubes. *Small*, 2009.

[48] D. P. Langley, M. Lagrange, G. Giusti, C. Jimnez, Y. Bréchet, N. D. Nguyen, and D. Bellet. Metallic nanowire networks: effects of thermal annealing on electrical resistance. *Nanoscale*, 2014.

[49] S. M. Ansar, F. S. Ameer, W. Hu, S. Zou, C. U. Pittman Jr., and D. Zhang. Removal of molecular adsorbates on gold nanoparticles using sodium borohydride in water. *NanoLetters*, 2013.

[50] H. Lu, D. Zhang, J. Cheng, J. Liu, J. Mao, and W. C. H. Choy. Locally welded silver nano-network transparent electrodes with high operational stability by a simple alcohol-based chemical approach. *Advanced Functional Materials*, 2015.

[51] B. Fultz and J. M. Howe. *Transmission Electron Microscopy and Diffractometry of Materials*. Springer-Verlag, Berlin Heidelberg, 2001.

7 Appendix

7.1 Silver nanocube synthesis

7.1.1 Materials and chemicals list

Equipment:

stirring hotplate with temperature controller (Heidolph MR Hei-Tec)
250 mL beaker
small beaker
10 new vials (⌀ 23 mm, 12 mL)
4 caps that loosely fit the vials (they should not close completely)
4 oval stir bars (6 x 15 mm)
crystallization dish
silicone oil (Sigma-Aldrich CAS 63148-62-9)
vial holder, custom made
rubber rings (inner diameter 18 mm)
micropipettes (Eppendorf Research plus)
pipette tips (Eppendorf, 0.5-10 μL, 10-100 μL, 100-1000 μL, 1-5 mL)
centrifuge tubes (BD Falcon, 14 mL)
centrifugator (Hettich Universal 320)
oven (Binder)
sonicator (Bransonic 2510E-MT)
filters (Merck Millipore, durapore membrane, 450, 220 and 100 nm)

Reagents:

polyvinylpyrrolidone, PVP (Aldrich CAS 9003-39-8, M_W = 55,000)
sodium hydrosulfide, NaSH (Sigma-Aldrich CAS 7647-01-0)
silvertrifluoroacetate, CF_3COOAg (Aldrich CAS 2966-50-9)
hydrogen chloride, HCl (Sigma-Aldrich CAS 7647-01-0, 37 % in water)
ethylene glycol, C_2H_6O (Fluka Analytical CAS 107-21-1)
ethanol
d.i. water
acetone
isopropanol

7.1.2 Reaction conditions and reproducibility

The growth of silver nanocubes is highly dependent on reaction conditions. The size of the vials and shape of the stir bars was seen to affect the result of the synthesis (using larger vials and rod-shaped stir bars did not yield cubes). The cleaning of the reaction vials and stir bars was done very carefully all times. We have observed that using a new HCl bottle altered our results slightly, hence the effect of reagent aging should be taken into consideration. Although keeping the exact same reaction conditions, we were not always able to reproduce the same result (see the images in figure 27 for example).

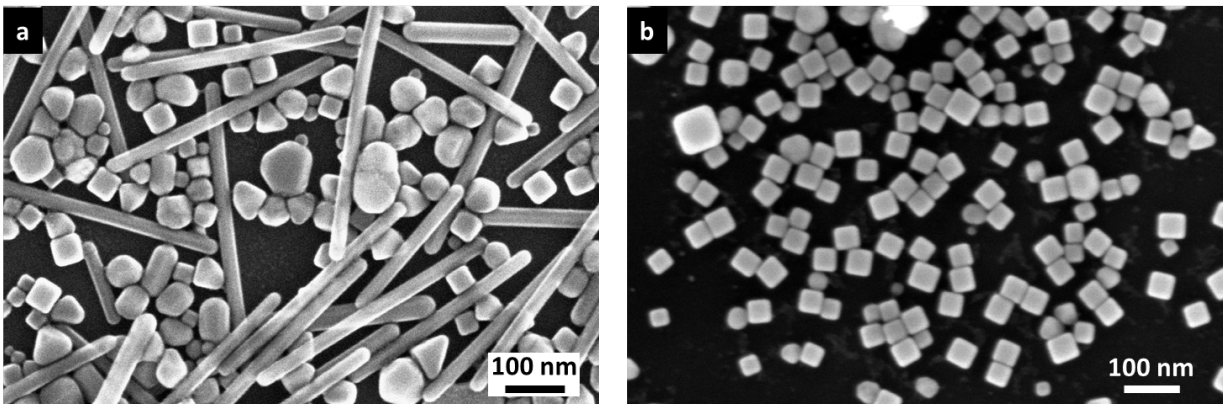

Figure 27: *Keeping, to our knowledge, all reaction conditions the same yielded wires the first time (a) and cubes the second time (b). The HCl concentration used was 0.21 mM.*

7.1.3 Non-cubic results

Several of our syntheses resulted in the formation of non cubic particles like wires, spherical particles and big rectangular blocks. Also clustering of silver and silverchloride was seen. Often the color of the end product revealed that the reaction had taken another route. When wires were accidentally made for example, the reaction looked light grey and upon shaking vortex like motions were visible. In some cases it was not possible to determine which parameter caused the distinct result. Next a few examples of undesired results with a known cause.

Accidentally using PVP with a smaller molecular weight (10,000 instead of 55,000) caused silver to grow into small and large shapeless particles that clustered together (see figure 28a). EDS scans performed on these clusters showed both a silver and a chlorine signal, indicating that part of the clusters consisted of AgCl. When using an HCl concentration that was ten times higher than normally, large rectangular blocks were formed (see figure 28b). Here too EDS showed both a silver and a chlorine signal. When investigating the effect of a low HCl concentration we fabricated spheres (see figure 29). The HCl concentration in this reaction was 0.055 mM.

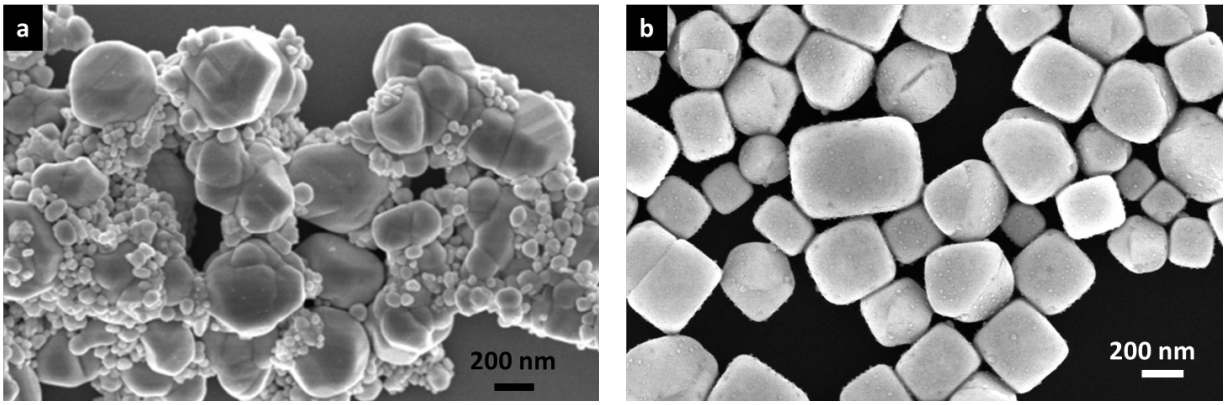

Figure 28: a: *SEM image of the result of a silver nanocube synthesis when accidentally PVP with a smaller chain length was used. The formation of one morphology (cubic) is lost and the particles cluster together.* **b:** *When accidentally using HCl at a ten times higher concentration, large rectangular blocks were formed. EDS showed that these particles consist of silverchloride.*

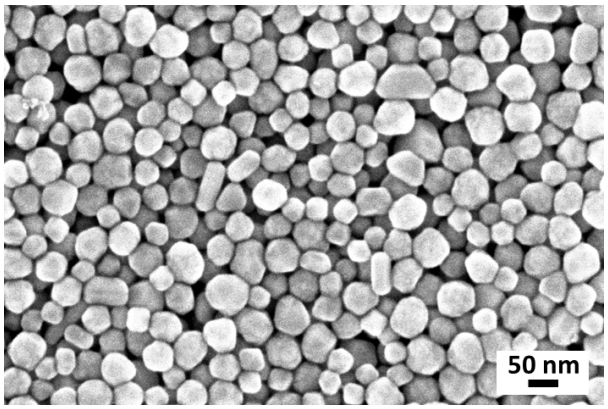

Figure 29: *When a very low HCl concentration was used (0.055 mM in the reaction), a silver nanocube synthesis yielded spherical particles.*

7.1.4 Size distribution of silver nanocubes

To determine the size distribution of the synthesized silver nanocubes, the imaging program ImageJ was used to convert a high resolution SEM image to a black and white image, as can be seen in figure 30. This program was then used to count the particles and measure their area, giving a size distribution. The overlay of images 30a and b is visible in figure 30c and shows that the image conversion slightly decreased the size of the particles.

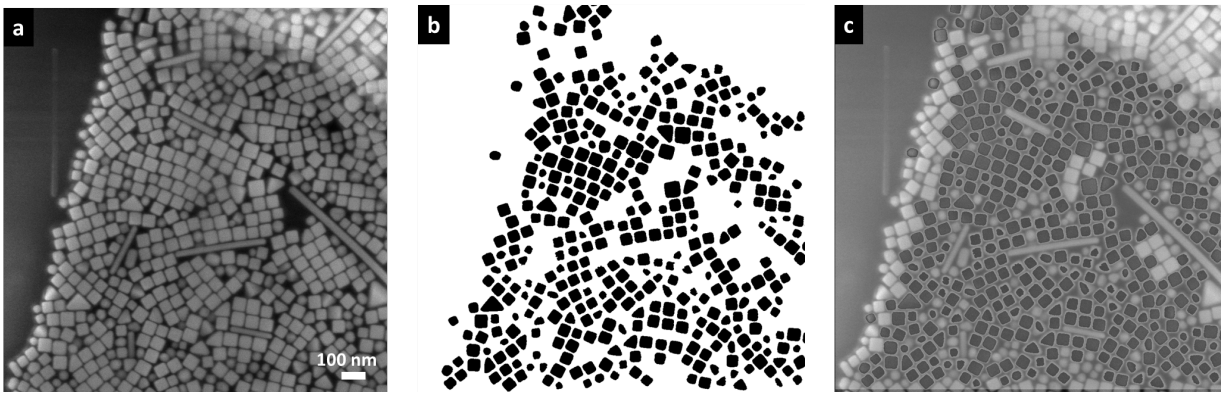

Figure 30: a: *An SEM image of silver nanocubes.* **b:** *The conversion of figure* **a** *to a black and white image using the imaging program ImageJ.* **c:** *The overlay of images* **a** *and* **b**. *This image reveils a mismatch of the particles' surface between the original image and its conversion. If the underestimation of the area is 10 %, the average cube will be 5.4 % larger in reality.*

7.2 Silicon wire template - preliminary result

For the fabrication of a PDMS mold with nanosize grid-shaped trenches a copper grid template on glass was used in this study. These copper wires were observed to vary in width, and their cross-section is curved. Therefore, an alternative process is currently investigated to produce a nanowire template. Figure 31 shows the preliminary result of a nanowire fabricated in silicon through electron beam lithography and plasma etching. The width of this wire is more constant and the cross-section more rectangular, as compared to the currently used copper wires. Once a PDMS mold is made from this new template, the effect of the improved trench shape on the assembly of nanocubes can be determined.

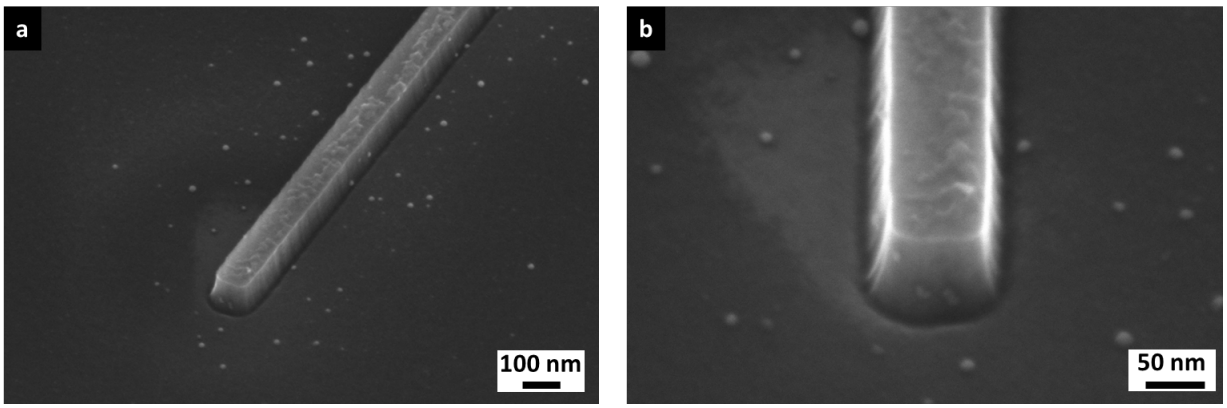

Figure 31: *Preliminary results of etching silicon to produce a wire template with less width variation and a more rectangular cross section than the evaporated chromium network used in this study. The height and width of this wire is 80 nm.* **a:** *SEM image, tilted 45 degrees (and rotated 30 degrees in comparison with* **b***).* **b:** *SEM image, tilted 45 degrees. This view shows the rectangular shape of the wire.*